Angular distortive matrices of phase transitions in the fcc-bcc-hcp system

Cyril Cayron

Laboratory of ThermoMechanical Metallurgy (LMTM), PX Group Chair, Ecole Polytechnique Fédérale de Lausanne (EPFL), Rue de la Maladière 71b, 2000 Neuchâtel, Switzerland. cyril.cayron@epfl.ch

Abstract: This work generalizes the one-step model previously developed on fcc→bcc martensitic transformations to the larger family of phase transitions in the fcc-bcc-hcp system. The angular distortive matrices are calculated for the bcc→fcc, bcc→hcp and fcc→hcp transitions, and for fcc→fcc mechanical twinning. The analytical expressions of the continuous atomic displacements, lattice distortion and lattice correspondence matrices result directly from the orientation relationships; the unique assumption is that the atoms are hard-spheres that can't interpenetrate each other. The displacive transformations occur in one-step by the change of the unique parameter which is the angle of distortion, without any defined intermediate phase or lattice shearing. The matrices of complete distortion form an algebra over the number field $\mathbb{Q}(\sqrt{6})$. The habit planes are predicted on the simple criterion that they are untilted by the distortion; the results are compared to experimental observations published in literature. Shuffle is required for bcc→hcp and fcc→hcp transitions because the hcp primitive Bravais lattice contains two atoms instead of one for the fcc and bcc phases; the analytical expressions of the shuffle trajectories are determined. Different crystallographic aspects are discussed. The steric barriers on dense planes are calculated and compared for fcc→fcc mechanical twining and fcc→bcc martensitic transformation. A distinction between the orientational and distortional variants is introduced, with an example given for the fcc→hcp transformation. Some crystallographic properties that could help the understanding of the transformation reversibility are also detailed. This approach is directly applicable to mechanical twinning in bcc and hcp crystals, and probably to diffusion-limited displacive transformations. This work gives a unified approach of the crystallography of displacive phase transformations and mechanical twinning in hard-sphere packed metallic alloys.

Keywords: Displacive transformations, twinning, angular distortive matrices, hard-sphere packing, habit plane.

1. Introduction

We have shown recently that it is possible to describe the fcc→bcc (face-centered cubic to body-centered cubic) martensitic transformation in steels and other iron alloys by a 3x3 matrix composed of terms that only depend on the angle of the lattice distortion [1][2]. In ref. [1], the matrix of complete distortion associated with the Pitch orientation relationship (OR) was calculated, and in ref. [2] the analytical expressions of the continuous distortion paths describing were given in the cases of Bain, Pitsch and Kurdjumov-Sachs (KS) ORs. A particular attention was paid to the distortion matrix associated with the KS

OR because it has two eigenvalues equal to 1, but is not an invariant plain strain and is not diagonalizable. It was shown that KS distortion matrix expressed in the reciprocal space has two untilted planes: the low-index $(\bar{1}11)_\gamma$ and the high-index $(\bar{2}25)_\gamma$ planes. Recent investigations have shown that associating variants by twin pairs allows changing the untilted $(\bar{2}25)_\gamma$ plane into a fully invariant strain plane [3]. The $\{225\}_\gamma$ habit planes (HPs) are widely observed in many steels and largely reported in literature. The fact that they result from a direct calculation, contrarily to the previous works implying complex double shear combinations, made us optimistic on the potentiality of the model. Since the hypotheses are reduced to assume the final OR and consider the atoms as hard-spheres, it is legitimate to ask whether the approach can be generalized to hexagonal close-packed (hcp) and mechanical twinning. This question is important because it would allow us to build a unified crystallographic model for the transitions and mechanical twinning in the wide family of phase transitions between hard-sphere packed phases, i.e. between fcc, bcc and hcp phases, as those that occur in various metallic alloys such as Fe, Ti, Zr, Co etc.

The link between of the phase transitions in the fcc-hcp-bcc system was foreseen in 1934 when Burgers could determine the OR related to the bcc-hcp phase transition [4]. Indeed, Burgers noticed that the bcc-hcp OR he could observe in zirconium was in full agreement with the KS OR reported for the fcc→bcc transformations in steels and with the OR reported for the fcc→hcp transformations in cobalt (Fig. 1a). This led him to propose a hypothesis in which the bcc-hcp transformation occurs in two steps, a bcc→fcc step followed by a fcc→hcp step. However, Burgers was not fully convinced and wrote: "*Whether in reality transformation of bcc into a hcp zirconium occurs via an intermediate fcc structure remains doubtful*". History is facetious because a similar hypothesis implying an intermediate phase was raised by us few years ago [5] (ignoring at that time the details of the Burgers' paper) but for the fcc→bcc transformation in martensitic steels, and the hypothetical intermediate phase was hcp. The supposition of an intermediate hexagonal phase in steels was also made more recently from transmission electron microscopy observations of extra spots in selected area diffraction patterns [6], but they actually come from twins artifacts [7]. Essentially, all the "two-step" models in the fcc-hcp-bcc Burgers triangle trying to explain a transformation $x \rightarrow z$ as a sequence of the two other transformations in the triangle, $x \rightarrow z = x \rightarrow y \rightarrow z$, with *x*, *y* and *z* being distinct phases in the set {fcc, hcp, hcp}, seems to be condemned to go in circle (we should say "in triangle"). However, such attempts come from a glimpse or from an intimate conviction that a strong structural link should exist between all the transitions implying the fcc, hcp and bcc phases. If one excludes the closed circuit models implying the intermediate phases, such a link remains to be found. The aim of the present paper is to propose a solution by generalizing the work performed for the fcc→bcc transition and the use of the angular distortive matrices. It will be shown that a 3x3 angular distortive matrix can be associated at each arrow (phase transition) in the Burgers triangle. The method can be also applied to the circular arrows at the three corner of the Burgers triangle, i.e. to twinning in each fcc, bcc or hcp phase.

All the possible transitions and twinning modes can't be detailed here, and the present work will report the calculations only for the fcc→fcc twinning, and for fcc→hcp, bcc→fcc and bcc→hcp transformations. The method can be applied to the twinning in the bcc and hcp systems, or to the hcp→bcc and hcp→fcc transitions, but these cases will not be detailed here because the bcc and hcp twin modes are numerous

and the two transitions are less common. Before presenting the calculations, let us give a brief literature review of the existing models.

Fcc→fcc twinning encompasses different mechanisms that should be distinguished. Annealing twins are created at high temperatures during recrystallization. They are formed along straight {111} planes "by accident" during the nucleation and growth of new grains because the $\Sigma 3$ twin boundaries have a low energy. Generally, all the four $\Sigma 3$ variants are formed, and the process can repeat itself which generates $\Sigma 3^n$ twins [8][9]. At medium and room temperatures, narrow twinned bands, called microtwins, can also form under strains. It is usually assumed that these microtwins are the consequence of regular creations and synchronized displacements of Shockley partial dislocations on the close-packed {111} planes transforming the ABCABC stacking into an ACBACB twinned stacking. This scenario seems in agreement with in-situ Transmission Electron Microscopy (TEM) observations, but the exact mechanism at the origin of the twinning dislocations is not yet fully understood. It is believed to occur via a pole mechanism, initially proposed by Cottrell and Bilby for twinning in bcc crystals [10]: a screw dislocation spirals around a pole and allows a layer-by-layer shearing on adjacent parallel planes [11]. However, to our knowledge, no spiraling dislocations in microtwins could have been evidenced, and recent TEM observations in Cu nano-alloys show that grain boundaries could be actually the sources of the Shockley partial dislocations [12]. Microtwinning is an important mode of deformation in the Twinning Induced Plasticity (TWIP) and Transformation Induced Plasticity (TRIP) steels [13][14]. At very low temperatures, large mechanical twins can also appear massively under strains by bursts producing load instability. These macrotwins propagates at speeds close to the speed of sound; which gives rise to audible clicks (twinning "cry"), as clearly shown by Blewitt *et al* [15] in Cu-8%Al single crystal deformed at 4.2K (their study is also reported in [16]). It is difficult to understand how a pole mechanism could be in agreement with such high speeds. Actually, it is probable that the mechanical twins result from a collective motion of the atoms similarly as for fcc-bcc martensitic transformation. In that assumption, the atoms would move cooperatively in one step. All the classical approaches of the lattice distortion by displacive transformation as macrotwinning and martensitic transformation are based on shears [17]-[21]; but, the crystallographic link between the shear distortion and the pole mechanisms was not clearly established. Moreover, simple shear is incompatible with the size of the atoms in a hard-sphere model (Supplementary Material S1). This is one of the reasons that led us to introduce the angular distortive matrices and use them to describe in one step the fcc-bcc transformations [2]. It will be shown in section 3 that it is possible to define fcc→fcc mechanical macrotwinning by using angular distortive matrices exactly as it was done for fcc→bcc martenstic transformations [2]. Although fcc→fcc macrotwinning is not very important in metallurgy because it occurs at very low temperatures, the comparison with fcc→bcc martensitic transformations is worth being explained; moreover, the results will be used to help the calculations for the other transitions.

Fcc→hcp transformations occur in cobalt alloys at temperatures which depends strongly on the alloy composition [21]-[23], and also in some Fe-Cr-Ni stainless steels quenched at low temperatures [24][25], and in some Mn-rich steels with shape memory properties [26]. The crystallographic explanations of the transformation given in metallurgy rely on arguments very similar to those used for fcc microtwinning: regular arrays of Shockley partial dislocations gliding on the $\{111\}_\gamma$ planes change the ABCABC stacking order of the fcc phase into the ABABAB order of the hcp phase. However, to our knowledge, there is no

consensus on the exact sequence of creation, dissociation and glide of dislocations at the origin of the nucleation and growth of the hcp phase [21][22]. A completely different model was proposed by the physicists P. Toledano *et al*. [27]. In their model, both the fcc and hcp structures in cobalt result from a "reconstructive" ordering mechanism of a disordered latent polytypic structure (for physicists the term "reconstructive" is not synonymous of "diffusive", see section 7.1). To our point of view, none of the explanations are totally satisfactory. The models based on coordinated creation and displacements of partial dislocations are not compatible with the high speeds of martensitic transformations; and the model based on the intermediate latent lattice does not take into account the atom size to explain how the atoms could move during the fcc→hcp reordering process. As for fcc→bcc displacive transformation and as for mechanical twinning, it will be shown in section 4 that it is possible to define bcc→fcc displacive transformations without coordinated motions of dislocations and without latent lattice, but by using angular distortive matrices.

Bcc→fcc transformations is the reverse transformation of the fcc→bcc martensitic transformation in steels; it can be obtained by heating martensitic steels to produce reverse austenite [28][29]. It can also be encountered by cooling Fe-Cr-Ni duplex steels in which δ ferrite decomposes into lath and spearhead isolated austenite [30], or in Widmanstätten austenite at the δ grain boundaries [31]. Bcc→fcc transformations are also widely studied in Cu-Zn brass and other Cu-Al, Cu-Sn alloys. The bcc phase orders itself during cooling and transforms into a B2 structure. The B2 phase undergoes a martensitic transformation by cooling below room temperature to form a monoclinic 9R structure which can be seen as a slightly distorted form of a polytype of the fcc (3R) phase [32]-[34]. In all these cases, the parent bcc and daughter fcc phases are in KS OR. Most often in literature the fcc or 9R daughter phase are created by thermal decomposition during an homogenisation at high temperature in the bcc domain (800-900°C) followed by a thermal treatment at medium temperature (300-500°C) [35]-[37]. The bcc→fcc or bcc→9R transformation also occurs under strain and is at the origin of shape memory effects [32][33][37]. To our knowledge, there is no alloy in which pure martensitic fcc phase is formed under cooling. However, the ideal case where the atoms would move collectively from a bcc to a fcc structure will be considered and the corresponding angular distortion matrices will be calculated in section 5. The validity of such an approach will be discussed in section 7.6.

Bcc→hcp transformations occur in Ti alloys and Zr alloys; the former are widely used in aerospace, medical and sport industries [38], and the latter for fuel cladding in nuclear reactors [39]. The crystallography of the bcc→hcp transformation in zirconium has been investigated by Burgers in 1934 [4] and his model is an important reference in metallurgy, such as the Bain model [40] for fcc→bcc transformations. As mentioned at the beginning of this introduction, Burgers was not convinced by the two-step bcc→fcc→hcp hypothesis, so he proposed the famous Burgers' model that combines a shear parallel to a $\{112\}_{bcc}$ plane in a $<111>_{bcc}$ direction with a shuffle and a homogeneous contraction of the lattice. This lattice distortion can be obtained by considering an orthorhombic superlattice close to the hcp and bcc lattices; which is used by Bowles and Mackenzie in the PTMC calculations to predict the HPs [41], and later by other researchers [42][43]. Another approach based on the edge-to-edge matching (E2EM) model has also been proposed by Zhang *et al.* [44]. In the Burger's paper one can figure out the atomic correspondence between the initial and final states; however, it is possible to improve the model by introducing the fact that the atoms are

hard-spheres and by merging the discontinuous steps into a continuous mechanism. It will be shown in section 6 that an angular distortion matrix can be used to model the bcc→hcp transformation in one-step, avoiding combining series of mechanisms as shear, dilatation, or using superstructures such as the orthorhombic lattice introduced in PTMC (equivalent to the Bain lattice).

The paper is thus built as follows: the sections 3 to 6 are dedicated to fcc→fcc twinning, and fcc→hcp, bcc→fcc and bcc→hcp transformations, respectively. Each section obeys the same scheme: a) the matrix of complete transformation is calculated from the OR, then b) the analytical expression of the continuously distorted lattices and atomic displacements are determined; shuffle is calculated when required, and c) the HPs are calculated without any free parameter and briefly compared to experimental literature. The style is voluntarily repetitive in order to point out the similarities of the transformations. The sections 3 to 6 can be read separately depending on the reader interest. The sections devoted to the calculations of the continuous intermediate states can be skipped at the first reading. The main ideas of the model and their consequences in term of qualitative understanding and quantitative predictability are discussed in section 7.

2. Notations and elementary formulae

Let us call $\mathbf{B}_0^\gamma = (\mathbf{a}_0^\gamma, \mathbf{b}_0^\gamma, \mathbf{c}_0^\gamma)$ with $\mathbf{a}_0^\gamma = [100]_\gamma$, $\mathbf{b}_0^\gamma = [010]_\gamma$, $\mathbf{c}_0^\gamma = [001]_\gamma$, the reference basis of the γ phase. The distortion matrix can be calculated by finding a primitive basis of the parent phase and by following how this basis is transformed during the transformation. Let us call $\mathbf{B}_p^\gamma$ this starting primitive basis, and $\mathbf{B}_p^{\gamma'}$ its image by distortion. When the transformation is complete, this basis becomes a basis of the daughter phase α. The initial and distorted bases are expressed by the matrices $\mathbf{B}_p^\gamma = \left[\mathbf{B}_0^\gamma \rightarrow \mathbf{B}_p^\gamma\right]$ and $\mathbf{B}_p^{\gamma'} = \left[\mathbf{B}_0^\gamma \rightarrow \mathbf{B}_p^{\gamma'}\right]$, respectively. The distortion matrix expressed in the initial primitive basis is then given by $\mathbf{D}_p^{\gamma\rightarrow\alpha} = \left[\mathbf{B}_p^\gamma \rightarrow \mathbf{B}_p^{\gamma'}\right] = \left[\mathbf{B}_p^\gamma \rightarrow \mathbf{B}_0^\gamma\right]\left[\mathbf{B}_0^\gamma \rightarrow \mathbf{B}_p^{\gamma'}\right] = \left(\mathbf{B}_p^\gamma\right)^{-1}\mathbf{B}_p^{\gamma'}$. In the reference basis of the parent phase it is

$$\mathbf{D}_0^{\gamma\rightarrow\alpha} = \left[\mathbf{B}_0^\gamma \rightarrow \mathbf{B}_p^\gamma\right]\mathbf{D}_p^{\gamma\rightarrow\alpha}\left[\mathbf{B}_p^\gamma \rightarrow \mathbf{B}_0^\gamma\right] = \mathbf{B}_p^{\gamma'}\left(\mathbf{B}_p^\gamma\right)^{-1} \qquad (1)$$

Formula (1) will be used to calculate the distortion matrix when the images of the vectors of the primitive lattice are known in the reference basis of the parent phase. If these images are known only in the reference basis of the daughter phase $\mathbf{B}_p^\alpha$, it is possible to convert them into the initial system by writing

$$\mathbf{B}_p^{\gamma'} = \mathbf{T}_0^{\gamma\rightarrow\alpha}\mathbf{B}_p^\alpha \qquad (2)$$

where $\mathbf{T}_0^{\gamma\rightarrow\alpha}$ is the matrix of change of coordinates which gives the coordinates of the vectors of the reference basis $\mathbf{B}_0^\alpha$ of the α crystal in the reference basis $\mathbf{B}_0^\gamma$ of the γ crystal:

$$\mathbf{T}_0^{\gamma\rightarrow\alpha} = \left[\mathbf{B}_0^\gamma \rightarrow \mathbf{B}_0^\alpha\right] \qquad (3)$$

This matrix can be determined from the OR by using an orthonormal basis common to the parent and daughter crystals, as explained for example in ref. [1] and detailed latter. Equations (1) and (2) will be used to determine the distortion matrix of the complete transformation. For the intermediate states, the calculations are similar but the size of the atoms will be taken into account to avoid their interpenetration.

In this paper, the fcc phase will be noted γ, the bcc phase α, and the hcp phase ε, i.e. fcc = γ, bcc = α and hcp = ε, as it is usually done for steels. Thus, we will not respect the usual notation used for brasses (bcc = β, fcc = α), and for titanium and zirconium (bcc = β, hcp = α). The directions and planes of the hcp phase will be written with three-index notation. As already assumed in ref. [1] and [2] for steels, the metal atoms are considered as hard spheres of same diameter in the three phases, which implies that:

$$\sqrt{2}\, a_\gamma = \sqrt{3}\, a_\alpha = 2a_\varepsilon = \sqrt{(3/2)}\, c_\varepsilon \qquad (4)$$

The ORs that will be used for the fcc-hcp-bcc transformations are the ORs corresponding to the Burgers triangle of Fig. 1a; they are the most commonly reported in literature. They are usually named by the initials of the discoverers: Kurdjumov-Sachs (KS) [45] for fcc→bcc (actually discovered by Young [46] in iron meteorites few years before Kurdjumov and Sachs), Burgers [4] for bcc→hcp, and Shoji-Nishiyama (SN) [47] for fcc→hcp. These ORs respect the parallelism of the close-packed directions (Fig. 1b). They are

- KS: $[110]_\gamma = [111]_\alpha$ and $(\bar{1}11)_\gamma // (\bar{1}10)_\alpha$ (5)
- Burgers: $[111]_\alpha = [100]_\varepsilon$ and $(\bar{1}10)_\alpha // (001)_\varepsilon$
- SN : $[110]_\gamma = [100]_\varepsilon$ and $(\bar{1}11)_\gamma // (001)_\varepsilon$

Other symmetrically equivalent planes and directions could have been chosen, for example $[\bar{1}10]_\gamma = [\bar{1}11]_\alpha$ and $(111)_\gamma // (110)_\alpha$ for KS, but the ORs (5) have been chosen to be coherent with our earlier works [2]. A coordinate change between the ORs is proposed in the end note 1.

It is possible to build a unique orthonormal basis $\mathbf{B}_c$ common to the fcc, bcc and hcp crystals. The first vector of this basis is the common close-packed direction; and the third vector is the normal to the common close-packed plane. The second vector is normal to these two vectors and its direction is chosen such that the basis $\mathbf{B}_c$ is right-hand. The basis $\mathbf{B}_c$ in each reference basis is

- $\left[\mathbf{B}_0^\gamma \rightarrow \mathbf{B}_c\right] = \frac{1}{a_\gamma}\begin{bmatrix} 1/\sqrt{2} & 1/\sqrt{6} & 1/\sqrt{3} \\ 1/\sqrt{2} & -1/\sqrt{6} & -1/\sqrt{3} \\ 0 & 2/\sqrt{6} & -1/\sqrt{3} \end{bmatrix}$
- $\left[\mathbf{B}_0^\alpha \rightarrow \mathbf{B}_c\right] = \frac{1}{a_\alpha}\begin{bmatrix} 1/\sqrt{3} & 1/\sqrt{6} & -1/\sqrt{2} \\ 1/\sqrt{3} & 1/\sqrt{6} & 1/\sqrt{2} \\ 1/\sqrt{3} & -2/\sqrt{6} & 0 \end{bmatrix}$ (6)
- $\left[\mathbf{B}_0^\varepsilon \rightarrow \mathbf{B}_c\right] = \frac{1}{a_\varepsilon}\begin{bmatrix} 1 & 1/\sqrt{3} & 0 \\ 0 & 2/\sqrt{3} & 0 \\ 0 & 0 & \sqrt{3/8} \end{bmatrix}$

These matrices and the theoretical ratios of the lattice parameters given in equation (4) allow the calculation of the coordinate transformation matrices between the fcc, bcc and hcp crystals. For example, $\mathbf{T}_0^{\gamma\to\alpha} = \left[\mathbf{B}_0^{\gamma} \to \mathbf{B}_0^{\alpha}\right] = \left[\mathbf{B}_0^{\gamma} \to \mathbf{B}_{\mathrm{c}}\right]\left[\mathbf{B}_{\mathrm{c}} \to \mathbf{B}_0^{\alpha}\right] = \left[\mathbf{B}_0^{\gamma} \to \mathbf{B}_{\mathrm{c}}\right]\left[\mathbf{B}_0^{\alpha} \to \mathbf{B}_{\mathrm{c}}\right]^{-1}$. Their values are reported in Table 1. It can be checked that the circular products is equal to the identity matrix. For example,

$$\mathbf{T}_0^{\gamma\to\alpha}\,\mathbf{T}_0^{\alpha\to\varepsilon}\,\mathbf{T}_0^{\varepsilon\to\gamma} = \mathbf{I} \tag{7}$$

where **I** is the identity matrix.

The coordinate transformation matrix $\mathbf{T}_0^{\alpha\to\gamma}$ can be used to write in the reference basis $\mathbf{B}_0^{\alpha}$ of the α daughter phase the images of the directions $\mathbf{a}_0^{\gamma} = [100]_{\gamma}$, $\mathbf{b}_0^{\gamma} = [010]_{\gamma}$, $\mathbf{c}_0^{\gamma} = [001]_{\gamma}$ distorted by $\mathbf{D}_0^{\gamma\to\alpha}$. The set of images forms the "correspondence" matrix, noted $\mathbf{C}_0^{\gamma\to\alpha}$, given by

$$\mathbf{C}_0^{\alpha\to\gamma} = \mathbf{T}_0^{\alpha\to\gamma}\mathbf{D}_0^{\gamma\to\alpha} = \left(\mathbf{T}_0^{\gamma\to\alpha}\right)^{-1}\mathbf{D}_0^{\gamma\to\alpha} \tag{8}$$

For example, in the case of the fcc→bcc distortion $\mathbf{D}_0^{\gamma\to\alpha}$ given in ref. [2], the correspondence matrix is a fcc→bcc Bain matrix:

$$\mathbf{C}_0^{\alpha\to\gamma} = \begin{bmatrix} 0 & 1 & 1 \\ 1 & 0 & 0 \\ 0 & 1 & -1 \end{bmatrix} \tag{9}$$

The correspondence matrix $\mathbf{C}_0^{\alpha\to\gamma}$ is used to calculate the images of the directions by distortion expressed in daughter reference basis. The images of the planes expressed in daughter reference basis are given by the correspondence matrix expressed in the reciprocal space, i.e. $\left(\mathbf{C}_0^{\alpha\to\gamma}\right)^{*} = \left(\mathbf{C}_0^{\alpha\to\gamma}\right)^{-T}$.

Let us recall briefly how the matrices should be used. A vector of **u** the direct space expressed in the reference basis $\mathbf{B}_0^{\gamma}$ as $\mathbf{u}_0^{\gamma}$ is written in the reference basis $\mathbf{B}_0^{\alpha}$ by $\mathbf{u}_0^{\alpha} = \mathbf{T}_0^{\alpha\to\gamma}\mathbf{u}_0^{\gamma}$. It should be understood that in this case the vector u does not change; it is just its coordinates that are recalculated. In order to obtain the coordinates of the image by distortion of the vector u expressed in basis of the parent phase $\mathbf{B}_0^{\gamma}$, one must use the distortion matrix: $\left(\mathbf{u}_0^{\gamma}\right)' = \mathbf{D}_0^{\gamma\to\alpha}\mathbf{u}_0^{\gamma}$. This image can be expressed in the reference basis of the daughter phase $\mathbf{B}_0^{\alpha}$: $(\mathbf{u}_0^{\alpha})' = \mathbf{C}_0^{\gamma\to\alpha}\mathbf{u}_0^{\gamma}$. We point out that the index 0 means the reference basis, but this basis is by default $\mathbf{B}_0^{\gamma}$ for $\mathbf{u}_0^{\gamma}$, and $\mathbf{B}_0^{\alpha}$ for $\mathbf{u}_0^{\alpha}$. When required the basis will be specified by unambiguously writing $\mathbf{u}_{/B_1}^{\alpha}$ to specify that the vector **u** of the phase α is expressed in the basis $\mathbf{B}_1$. The same equalities hold for the vectors **g** of the reciprocal space if one replaces the matrices by their "star", i.e. the inverse of the transpose.

The HPs will be calculated from the same criterion as in [2]. They correspond to the planes **g** untilted by the distortion matrix **D**. The amplitude of the tilt is given by the part $\Delta\mathbf{g}_{\perp}$ of the displacement $\Delta\mathbf{g}$ perpendicular to **g** , with $\Delta\mathbf{g}$ = **g**'- **g** , and **g**' = $\mathbf{D}^{*}$**g**, where $\mathbf{D}^{*}$ is the distortion matrix expressed in the reciprocal space (it is the inverse of the transpose of **D**). The untilted plane is thus given by

$$\left\|\Delta\mathbf{g}_{\perp}\right\| = 0\text{, or equivalently, } \mathbf{g} \text{ is an eigenvector of } \mathbf{D}^{*} \qquad (10)$$

The amplitudes of $\Delta\mathbf{g}_{\perp}$ can be plotted in 2D as a function of the spherical coordinates of **g**, and the untilted planes are given by the zero values numerically deduced from the 2D graph [2]. The exact values of **g** can be determined by calculating the eigenvectors of $\mathbf{D}^{*}$. For example, the exact values of the $(\bar{2}25)_{\gamma}$ HP obtained from $\mathbf{D}^{*}$ corresponding to the KS OR is actually $(\bar{1}1\sqrt{6})_{\gamma}$. Both numerical 2D graphs of $\left\|\Delta\mathbf{g}_{\perp}\right\|$ and exact calculations will be presented in the paper.

The calculated HPs will be compared with the experimental ones reported in literature. The equivalent symmetries of the parent and daughter phases may make this comparison difficult. Therefore, in order to keep the coherency of notation in the whole paper, when possible, the ORs and corresponding HPs reported in literature will be written according to the choice of equation (5).

3. FCC→FCC mechanical twinning

3.1. Matrix of complete lattice distortion

As for fcc→bcc transformations [1][2], we choose $(\bar{1}11)_{\gamma}$ to be the untilted plane. For twinning, this plane is actually fully invariant. The reference frame and the positions of the atoms in the initial fcc state are shown in Fig. 2a and Fig. 3b. The triangle POK is unchanged by twinning (β=60°), contrarily to what happens in the fcc→bcc transformation. The atom in M, initially such that **PM** = $[100]_{\gamma}$, moves and passes over the two atoms in O and K, and, after twinning, in its final position, M is located such that the tetrahedron POKM is regular. The complete lattice distortion can be determined by considering that the vectors **x** = **PO** =½ $[110]_{\gamma}$ and **y** = **PK** =½ $[101]_{\gamma}$ are invariant, and that the vector **z** = **PM** = 1/3 $[211]_{\gamma}$ + 1/3 $[1\bar{1}\bar{1}]_{\gamma}$ = $[100]_{\gamma}$ is transformed into the vector **PM'** = 1/6 $[211]_{\gamma}$ +1/3 $[1\bar{1}\bar{1}]_{\gamma}$ = 1/6 $[4\bar{1}\bar{1}]_{\gamma}$. This means that

$$\mathbf{B}_{p}^{\gamma} = \begin{bmatrix} 1/2 & 1/2 & 1 \\ 1/2 & 0 & 0 \\ 0 & 1/2 & 0 \end{bmatrix} \text{ and } \mathbf{B}_{p}^{\gamma'} = \begin{bmatrix} 1/2 & 1/2 & 4/6 \\ 1/2 & 0 & -1/6 \\ 0 & 1/2 & -1/6 \end{bmatrix}\text{, and thus, by using formula (1),}$$

$$\mathbf{D}_{0}^{\gamma\to\gamma} = \mathbf{B}_{p}^{\gamma'}\left(\mathbf{B}_{p}^{\gamma}\right)^{-1} = \frac{1}{6}\begin{bmatrix} 4 & 2 & 2 \\ -1 & 7 & 1 \\ -1 & 1 & 7 \end{bmatrix} \qquad (11)$$

The twinning correspondence matrix $\mathbf{C}_{0}^{\gamma\to\gamma}$ can be calculated thanks to equation (8) and to the coordinate transformation matrix:

$$\mathbf{T}_{0}^{\gamma\to\gamma} = \frac{1}{3}\begin{bmatrix} 1 & 2 & 2 \\ 2 & 1 & -2 \\ 2 & -2 & 1 \end{bmatrix} \qquad (12)$$

$$\mathbf{C}_0^{\gamma\to\gamma} = \mathbf{T}_0^{\gamma\to\gamma}\mathbf{D}_0^{\gamma\to\gamma} = \frac{1}{2}\begin{bmatrix} 0 & 2 & 2 \\ 1 & 1 & -1 \\ 1 & -1 & 1 \end{bmatrix} \quad (13)$$

It can be checked by using $\mathbf{T}_0^{\gamma\to\gamma}$ that the vector $[\bar{1}11]_\gamma$ in the parent crystal is at the place of the $[1\bar{1}\bar{1}]_\gamma$ vector in the reference basis of the twinned crystal, which does not mean that the distortion preserves this vector. Indeed, it can be checked by using $\mathbf{C}_0^{\gamma\to\gamma}$ that the vector $[\bar{1}11]_\gamma$ is actually transformed into ½ $[4\bar{1}\bar{1}]_\gamma$. It can also be checked by using $\left(\mathbf{C}_0^{\gamma\to\gamma}\right)^*$ that the $(\bar{1}11)_\gamma$ plane once distorted becomes the $(1\bar{1}\bar{1})_\gamma$ plane of the twinned crystal.

3.2. Matrix of continuous lattice distortion

The matrix (11) gives the complete twinning distortion of the fcc lattice. It is possible to determine all the continuous intermediate states by considering that the atoms are hard-spheres that "roll" on each other. Let us call η the angle (**JH**, **JM**), i.e., the angle between the $(\bar{1}11)_\gamma$ and $(111)_\gamma$ planes. For fcc twinning the deformation occurs such that $\mathrm{JP} = \mathrm{JM} = {\sqrt{3}}/{2}\, d$ where *d* is the atom diameter, thus $JP = JM = {\sqrt{6}}/{4}\, a_\gamma$.

Since the triangle PJM remains isosceles during the distortion, the angle η is such that η = 2γ (here the angle γ should not be confused with the fcc γ phase), as represented in Fig. 2b and Fig. 3b.

During the displacement of the atom is M, the angle η varies from η = arcos(1/3) = 70.5° to η = - arcos(1/3) = 180°-70.5° = 109.5°. It is important to notice that this is obtained by the same displacement of the atom in M as for the fcc→bcc transformation [2] except now that the angle β remains fixed at 60°, which means that the atom in M has to pass over the two atoms in O and K such that the distance OK remains constant and equal to *d*, whereas in the fcc→bcc martensite transformation this distance increases by the opening of the angle (**PO**, **PK**) from 60° to 70.5°. Therefore, equation (21) of ref. [2] of fcc→bcc transformation can be modified in order to get its equivalent for fcc→fcc twinning. It becomes

$$\left[\mathbf{B}_s \to \mathbf{B}_p(\eta)\right] = \begin{bmatrix} 1 & \cos(\beta) & \cos(\gamma)\|\mathbf{z}\|\cos({\beta}/{2}) \\ 0 & \sin(\beta) & \cos(\gamma)\|\mathbf{z}\|\sin({\beta}/{2}) \\ 0 & 0 & \|\mathbf{z}\|\sin(\gamma) \end{bmatrix} \quad (14)$$

with β = 60°, η = 2γ and $\|\boldsymbol{z}\|$ the norm of the vector $\mathbf{z} = [100]_\gamma = \mathbf{PM}$. Equation (14) gives the evolution of the values of the basis $\mathbf{B}_p$ of the primitive lattice formed by the vectors **PO**, **PK** and **PM** during the distortion in reference to a fixed orthonormal basis $\mathbf{B}_s$ formed from the vectors **PO**, **PK** and **PM** in the initial fcc crystal.

Equation (14) can be written as function of the angle η only, by noticing that the part $\cos(\gamma)\|\boldsymbol{z}\|$ is the projection of **PM** on the line **PJ**, and thus is equal to $\mathrm{PJ}(1+\cos(\gamma))$, and that $\sin(\gamma)\|\boldsymbol{z}\| = PJ\sin(\eta)$, as illustrated in Fig. 2c. Therefore, equation (14) becomes:

$$\left[\mathbf{B}_s \rightarrow \mathbf{B}_p(\eta)\right] = \begin{bmatrix} 1 & 1/2 & \frac{3}{4\sqrt{2}}(1+\cos(\eta)) \\ 0 & \sqrt{3}/2 & \frac{\sqrt{3}}{4\sqrt{2}}(1+\cos(\eta)) \\ 0 & 0 & \frac{\sqrt{3}}{2\sqrt{2}}\sin(\eta) \end{bmatrix} \quad (15)$$

The lattice distortion matrix in the reference basis $\mathbf{B}_p$ (70.5°) is

$$\mathbf{D}_p^{\gamma\rightarrow\gamma}(\eta) = \left[\mathbf{B}_p(70.5°) \rightarrow \mathbf{B}_p(\eta)\right] = \left[\mathbf{B}_p(70.5°) \rightarrow \mathbf{B}_s\right]\left[\mathbf{B}_s \rightarrow \mathbf{B}_p(\eta)\right]$$

with $[\mathbf{B}_p(70.5°) \rightarrow \mathbf{B}_s] = [\mathbf{B}_s \rightarrow \mathbf{B}_p(70.5°)]^{-1}$ also given by equation (15) with η = 70.5°.

The coordinate transformation matrix from $\mathbf{B}_0^{\gamma}$ to $\mathbf{B}_p$ = (**PO**, **PK**, **PM**) in the initial fcc reference basis is:

$$\left[\mathbf{B}_0^{\gamma} \rightarrow \mathbf{B}_p(70.5°)\right] = \begin{bmatrix} 1/\sqrt{2} & 1/\sqrt{2} & 1 \\ 1/\sqrt{2} & 0 & 0 \\ 0 & 1/\sqrt{2} & 0 \end{bmatrix} \quad (16)$$

It is now possible to calculate the twinning lattice distortion in the reference basis $\mathbf{B}_0^{\gamma}$ by using formula (1):

$$\mathbf{D}_0^{\gamma\rightarrow\gamma}(\eta) = \left[\mathbf{B}_0^{\gamma} \rightarrow \mathbf{B}_p(70.5°)\right]\mathbf{D}_p^{\gamma\rightarrow\gamma}(\eta)\left[\mathbf{B}_0^{\gamma} \rightarrow \mathbf{B}_p(70.5°)\right]^{-1} \quad (17)$$

$$= \frac{1}{4}\begin{bmatrix} 2+2Y+\sqrt{2}\sqrt{1-Y^2} & 2-2Y-\sqrt{2}\sqrt{1-Y^2} & 2-2Y-\sqrt{2}\sqrt{1-Y^2} \\ 1+Y-\sqrt{2}\sqrt{1-Y^2} & 3-Y+\sqrt{2}\sqrt{1-Y^2} & -1-Y+\sqrt{2}\sqrt{1-Y^2} \\ 1+Y-\sqrt{2}\sqrt{1-Y^2} & -1-Y+\sqrt{2}\sqrt{1-Y^2} & 3-Y+\sqrt{2}\sqrt{1-Y^2} \end{bmatrix}$$

with Y = cos(η).

It can be checked that for the initial state, since η = 70.5°, Y = cos(η) = 1/3, $\mathbf{D}_0^{\gamma\rightarrow\gamma}(\eta = 70.5°)$ is the identity matrix, and that the complete distortion obtained for η = 180°-70.5°, Y = cos(η) = -1/3, leads to the matrix given in equation (11). This is the same expression as it could be found by a simple shear of amplitude *s* = 1/√2 on a $(\bar{1}11)_\gamma$ plane on the -$[211]_\gamma$ direction [53]. The interesting point here is that all the continuous intermediate states are calculated from equation (17), whereas a continuous simple shear is unrealistic due to the interpenetration of the atoms, i.e., the atom M displaced by shearing would collide with the atoms in O and K.

All the atoms M of the crystal move during the fcc→fcc twinning transformation exactly as the lattice:

$$\mathbf{PM'} = \mathbf{D}_0^{\gamma\rightarrow\gamma}(\eta)\,\mathbf{PM} \quad (18)$$

Therefore, as for fcc→bcc martensitic transformation, mechanical twinning does not require shuffle. The similarities and differences between these two types of transformation are visible by comparing the schemes of Fig. 3a and Fig. 3b, respectively.

3.3. Habit plane

The matrix $\mathbf{D}_0^{\gamma\to\gamma}$ gives the image $\mathbf{u'}_0^{\gamma}$ in the initial fcc basis $\mathbf{B}_0^{\gamma}$ of the direction $\mathbf{u}_0^{\gamma}$ by twinning:

$$\mathbf{u'}_0^{\gamma} = \mathbf{D}_0^{\gamma\to\gamma}\mathbf{u}_0^{\gamma} \tag{19}$$

The inverse of its transpose gives the images of the plane $\mathbf{g}_0^{\gamma}$:

$$\mathbf{g'}_0^{\gamma} = \left(\mathbf{D}_0^{\gamma\to\gamma}\right)^{*}\mathbf{g}_0^{\gamma} \text{ , with} \tag{20}$$

$$\left(\mathbf{D}_0^{\gamma\to\gamma}\right)^{*} = \left(\mathbf{D}_0^{\gamma\to\gamma}\right)^{-T} = \frac{1}{6}\begin{bmatrix} 8 & 1 & 1 \\ -2 & 5 & -1 \\ -2 & -1 & 5 \end{bmatrix} \tag{21}$$

It can be checked that the vector $\mathbf{g}^{\gamma}$ = $(\bar{1}11)_{\gamma}$ is the eigenvector vector of $\left(\mathbf{D}_0^{\gamma\to\gamma}\right)^{*}$ associated to the eigenvalue 1. This means that the plane $\mathbf{g}^{\gamma}$ is *globally* invariant, i.e. it is not tilted and its norm (interplanar spacing) is not changed. This condition is necessary but not sufficient to imply that that this plane is *fully* invariant. In order to check the full invariance condition one has to check that two non-parallel directions belonging to this plane are also invariant. It is the case here, but it should be noticed that it is not the case of the $(\bar{1}11)_{\gamma}$ plane distorted by the fcc→bcc martensitic transformations into the $(\bar{1}10)_{\alpha}$ plane [2].

4. FCC→ HCP transformation

4.1. Matrix of complete lattice distortion

In order to calculate the lattice distortion matrix, an intermediate primitive basis $\mathbf{B}_p^{\gamma}$ = (**x**, **y**, **z**)$_{\gamma}$ should be found. Clearly, since the vectors **PO** = ½ [110]$_{\gamma}$ and **PK** = ½ [101]$_{\gamma}$ are invariant, they can be chosen for the **x** and **y** axes, respectively, as for twinning. However, the vector **PM** cannot be taken for the **z** axis of the intermediate basis $\mathbf{B}_p^{\gamma}$ because the basis (**x**, **y**, **z**)$_{\gamma}$ and the distortion would be exactly the same as for twinning. It will be shown that the displacement of the atom in position M is actually a shuffle. Instead of choosing the atom M located on the $(\bar{1}11)_{\gamma}$ plane at the level *l = 1* (Fig. 3c), we choose the atom in N located at the upper level *l = 2*, i.e., such that **PN** = ½ $[2\bar{1}\bar{1}]_{\gamma}$. We point out here that contrarily to the primitive basis used for fcc→bcc transformations, the basis $\mathbf{B}_p^{\gamma}$ of this section contains not one, but two atoms. The vectors **PO** = ½ [110]$_{\gamma}$ and **PK** = ½ [101]$_{\gamma}$ of invariant plane $(\bar{1}11)_{\gamma}$ are invariant, and the vector **PN** = ½ $[2\bar{1}\bar{1}]_{\gamma}$ = 1/6 $[211]_{\gamma}$ + 2/3 $[1\bar{1}\bar{1}]_{\gamma}$ is transformed into the vector **PN'** = 2/3 $[1\bar{1}\bar{1}]_{\gamma}$. This means that

$\mathbf{B}_p^{\gamma} = \begin{bmatrix} 1/2 & 1/2 & 1 \\ 1/2 & 0 & -1/2 \\ 0 & 1/2 & -1/2 \end{bmatrix}$ and $\mathbf{B}_p^{\gamma'} = \begin{bmatrix} 1/2 & 1/2 & 2/3 \\ 1/2 & 0 & -2/3 \\ 0 & 1/2 & -2/3 \end{bmatrix}$, and thus, by using formula (1),

$$\mathbf{D}_0^{\gamma\to\varepsilon} = \mathbf{B}_p^{\gamma'}\left(\mathbf{B}_p^{\gamma}\right)^{-1} = \frac{1}{12}\begin{bmatrix} 10 & 2 & 2 \\ -1 & 13 & 1 \\ -1 & 1 & 13 \end{bmatrix} \quad (22)$$

The correspondence matrix $\mathbf{C}_0^{\varepsilon\to\gamma}$ is calculated thanks to equation (8) and the coordinate transformation matrix reported in Table 1. It is

$$\mathbf{C}_0^{\varepsilon\to\gamma} = \mathbf{T}_0^{\varepsilon\to\gamma}\mathbf{D}_0^{\gamma\to\varepsilon} = \frac{1}{2}\begin{bmatrix} 2 & 2 & 2 \\ 1 & -1 & 3 \\ 1 & -1 & -1 \end{bmatrix} \quad (23)$$

It can be checked by using $\mathbf{T}_0^{\varepsilon\to\gamma}$ (Table 1) that the vector $[\bar{1}11]_\gamma$ in the parent crystal is at the place of the 3/2 [001] vector in the reference basis of the hcp crystal, which does not mean that the distortion preserves the parallelism of this direction. Indeed, it can be checked by using $\mathbf{C}_0^{\varepsilon\to\gamma}$ that the vector $[\bar{1}11]_\gamma$ is actually transformed into ½ $[21\bar{3}]_\gamma$. It can also be checked by using $\left(\mathbf{C}_0^{\varepsilon\to\gamma}\right)^*$ that the 2/3 $(1\bar{1}\bar{1})_\gamma$ plane once distorted becomes the (001) plane of the hcp crystal.

4.2. Matrix of continuous lattice distortion

The matrix (22) gives the complete distortion of the fcc lattice. Here again, it is possible to determine all the intermediate states of the transformation by considering that the atoms are hard-spheres that "roll" on each other. During the fcc→hcp transformation the points P, O, K, I and J are fixed (Fig. 1a and Fig. 3c). The atom N has to jump above the two atoms located on the $(\bar{1}11)$ plane below. There are two possibilities for the atom located in M: it can jump above the atoms located in O and K, following the same trajectory as for the atom N, but relatively to the $(\bar{1}11)$ plane below, or it can remain in the same position. If the atom in M moves, its trajectory can be deduced from the calculations performed for twinning in the previous section. In the $\mathbf{B}_0^\gamma$ basis, the vector **JM** = ¼ $[2\bar{1}\bar{1}]_\gamma$ is transformed exactly as for twinning; it becomes the vector **JM'** = $\mathbf{D}_0^{\gamma\to\gamma}(\eta)$**JM** with $\mathbf{D}_0^{\gamma\to\gamma}(\eta)$ the matrix given in equation (17). The vector **IN** follow the same change as the vector **JM**, and thus **IN'** = $\mathbf{D}_0^{\gamma\to\gamma}(\eta)$**IN**. The vector **PN** is thus changed into **PN'** = **PI** + **IN'** = **PI** + $\mathbf{D}_0^{\gamma\to\gamma}(\eta)$**IN**. Therefore, the primitive basis $\mathbf{B}_p$ formed by the vectors **x** = **PO** = ½ $[110]_\gamma$, **y** = **PK** = ½ $[101]_\gamma$ and **z** = **PN = PI + IN**, with **PI** = 1/4 $[2\bar{1}\bar{1}]_\gamma$, takes the form of a matrix (**x**, **y**, **z**) that can be expressed directly in the $\mathbf{B}_0^\gamma$ basis by:

$$\left[\mathbf{B}_0^\gamma \to \mathbf{B}_p(\eta)\right] = \begin{bmatrix} 1/2 & 1/2 & 1/2 + \frac{1}{4}(2Y + \sqrt{2}\sqrt{1-Y^2}) \\ 1/2 & 0 & -1/4 + \frac{1}{4}(Y - \sqrt{2}\sqrt{1-Y^2}) \\ 0 & 1/2 & -1/4 + \frac{1}{4}(Y - \sqrt{2}\sqrt{1-Y^2}) \end{bmatrix} \quad (24)$$

with Y = cos(η).

The continuous lattice distortion matrix is deduced from formula (1); it is

$$\mathbf{D}_0^{\gamma\to\varepsilon}(\eta)=\left[\mathbf{B}_0^{\gamma}\to\mathbf{B}_p(70.5°)\right]\left[\mathbf{B}_p(\eta)\to\mathbf{B}_0^{\gamma}\right]^{-1} \qquad (25)$$
$$=\frac{1}{8}\begin{bmatrix} 6+2Y+\sqrt{2}\sqrt{1-Y^2} & 2-2Y-\sqrt{2}\sqrt{1-Y^2} & 2-2Y-\sqrt{2}\sqrt{1-Y^2} \\ 1+Y-\sqrt{2}\sqrt{1-Y^2} & 7-Y+\sqrt{2}\sqrt{1-Y^2} & -1-Y+\sqrt{2}\sqrt{1-Y^2} \\ 1+Y-\sqrt{2}\sqrt{1-Y^2} & -1-Y+\sqrt{2}\sqrt{1-Y^2} & 7-Y+\sqrt{2}\sqrt{1-Y^2} \end{bmatrix}$$

It can be checked that for the initial state, since η = 70.5°, Y = cos(η) = 1/3, $\mathbf{D}_0^{\gamma\to\varepsilon}(\eta=70.5°)$ is the identity matrix, and that the complete transformation matrix obtained for η = 180° - 70.5° = 109.5°, Y = cos(η)= -1/3 is the matrix (22).

4.3. Schuffle

All the atoms of type N = (*u*, *v*, *w*) located similarly as N in the plane $(\bar{1}11)$ of even layers, i.e., such that *l* = *(-u+v+w)* is even, have a trajectory that directly follows the lattice distortion:

$$\mathbf{PN'} = \mathbf{D}_0^{\gamma\to\varepsilon}(\eta)\,\mathbf{PN} \qquad (26)$$

All the other atoms of type M = (*u*, *v*, *w*) located similarly as M in the plane $(\bar{1}11)$ of odd layers, i.e., such that *l = (-u+v+w)* is odd, have a trajectory that does not follow the lattice distortion, but that can be deduced of it. There are two equivalent shuffles of the M atoms; they can be determined by considering the trajectories of M in its local unit cell. Either M does not move, or it moves as it would do for a twinning distortion. The origin P of the unit cell in which the atom M is located is deduced from M by the translation vector **t** = $[010]_\gamma$. Therefore, the trajectories of the atoms M that do not move in their unit cells obey the equation:

$$\underline{\text{Shuffle S0:}}\quad \mathbf{PM'} = \mathbf{D}_0^{\gamma\to\varepsilon}(\eta)\,(\mathbf{PM}\text{-}\mathbf{t}) + \mathbf{t}\,,\ \text{with } \mathbf{t} = [010]_\gamma \qquad (27)$$

And the trajectories of the atoms M that move by a local twinning displacement in their unit cells, as shown in Fig. 3c, obey the equation:

$$\underline{\text{Shuffle S2:}}\quad \mathbf{PM'} = \mathbf{D}_0^{\gamma\to\varepsilon}(\eta)\,(\mathbf{PM}\text{-}\mathbf{t}) + \mathbf{D}_0^{\gamma\to\gamma}(\eta)\,\mathbf{t}\,,\ \text{with } \mathbf{t} = [010]_\gamma \qquad (28)$$

These two trajectories (noted S0 and S2) do not have the same expression as for the other atoms of the lattice given by (26); they are shuffles. The need of shuffle comes from the fact that the primitive unit cell of the hcp structure contains two atoms; this also explains why we could not choose **PM** as **z** axis in the primitive basis $\mathbf{B}_p$ and thus justifies our choice of basis at the beginning of the section.

4.4. Habit plane

The matrix $\mathbf{D}_0^{\gamma\to\varepsilon}$ gives the images of the direction $\mathbf{u}_0^{\gamma}$ in the initial fcc basis $\mathbf{B}_0^{\gamma}$ by the fcc→hcp distortion. The inverse of its transpose gives the image of the plane $\mathbf{g}_0^{\gamma}$.

$$\mathbf{g'}_0^{\gamma} = \left(\mathbf{D}_0^{\gamma\to\varepsilon}\right)^{*}\mathbf{g}_0^{\gamma}\ ,\ \text{with} \qquad (29)$$

$$\left(\mathbf{D}_0^{\gamma\to\varepsilon}\right)^* = \left(\mathbf{D}_0^{\gamma\to\varepsilon}\right)^{-T} = \frac{1}{12}\begin{bmatrix} 14 & 1 & 1 \\ -2 & 11 & -1 \\ -2 & -1 & 11 \end{bmatrix} \quad (30)$$

It can be checked that the (reciprocal) vector $\mathbf{g}^\gamma$ = $(\bar{1}11)_\gamma$ is invariant by $\left(\mathbf{D}_0^{\gamma\to\varepsilon}\right)^*$, which means that this plane is globally invariant. It can be checked by $\mathbf{D}_0^{\gamma\to\varepsilon}$ and by choosing two non-parallel directions in $(\bar{1}11)_\gamma$ that this plane is actually fully invariant. Therefore, the $(\bar{1}11)_\gamma$ plane appears as the natural HP for fcc→hcp transformation.

The continuous analytical expressions of the angular distortive matrices of fcc→bcc transformations -equation (31) of ref. [2]-, of fcc→fcc macrotwinning -equation (17)-, and of fcc→hcp transformations -equation (25) with equation (27) for the shuffle-, have been introduced into a computer program written in VPython that allows representing the crystals in three dimensions. Simulation movies of the distortion of a fcc cube constituted by 6x6x6 unit cells transformed into bcc, fcc-twinned and hcp structures are given in Supplementary Materials S2, S3 and S4, respectively. The initial, intermediate and final states are represented in blue, yellow and red colors for fcc→bcc, fcc→fcc and fcc→hcp transformations, in Fig. 4a, b and c, respectively. The intermediate state is arbitrarily chosen at mid-path of the complete transformation.

5. BCC→FCC transformation

5.1. Matrix of complete lattice distortion

The OR between the bcc parent and fcc daughter phases are the KS OR of equation (5). The distortion matrix can be determined by considering that the vectors **x** = **PO**$_\alpha$ =½ $[111]_\alpha$ and **y** = **PK**$_\alpha$ =½ $[11\bar{1}]_\alpha$ of the bcc phase become by lattice distortion the vectors **PO**$_\gamma$ =½ $[110]_\gamma$ and **PK**$_\gamma$ =½ $[101]_\gamma$ of the fcc phase (Fig. 5 and Fig. 6a), and that the vector **PM**$_\alpha$ = $[010]_\alpha$ is transformed into the vector **z** = **PM**$_\gamma$ = $[100]_\gamma$. It implies that the primitive basis

$\mathbf{B}_p^\alpha = \begin{bmatrix} 1/2 & 1/2 & 0 \\ 1/2 & 1/2 & 1 \\ 1/2 & -1/2 & 0 \end{bmatrix}$ has for image in the basis of the product phase $\mathbf{B}_0^\gamma$, the basis $\mathbf{B}_{p/\gamma_0}^{\alpha'} = \begin{bmatrix} 1/2 & 1/2 & 1 \\ 1/2 & 0 & 0 \\ 0 & 1/2 & 0 \end{bmatrix}$.

This image can be calculated in the reference basis of the parent crystal $\mathbf{B}_0^\alpha$ by using the coordinate transformation matrix $\mathbf{T}_0^{\alpha\to\gamma}$ given in Table 1. It follows that $\mathbf{B}_p^{\alpha'} = \mathbf{T}_0^{\alpha\to\gamma}\mathbf{B}_{p/\gamma_0}^{\alpha'}$, and thus $\mathbf{D}_0^{\alpha\to\gamma} = \mathbf{T}_0^{\alpha\to\gamma}\mathbf{B}_{p/\gamma_0}^{\alpha'}\left(\mathbf{B}_p^\alpha\right)^{-1}$ becomes after calculations

$$\mathbf{D}_0^{\alpha\to\gamma} = \begin{bmatrix} \frac{3}{4}+\frac{\sqrt{6}}{24} & \frac{\sqrt{6}}{12} & \frac{1}{4}-\frac{\sqrt{6}}{8} \\ -\frac{1}{4}+\frac{\sqrt{6}}{24} & 1+\frac{\sqrt{6}}{12} & \frac{1}{4}-\frac{\sqrt{6}}{8} \\ \frac{1}{4}-\frac{\sqrt{6}}{12} & \frac{1}{2}-\frac{\sqrt{6}}{6} & \frac{1}{4}+\frac{\sqrt{6}}{4} \end{bmatrix} \quad (31)$$

Another way to find this result is to use the complete distortion matrix of the fcc→bcc transformation $\mathbf{D}_0^{\gamma\to\alpha}$ reported in equation 32 of ref. [2], and notice that

$$\mathbf{D}_0^{\alpha\to\gamma} = \mathbf{T}_0^{\alpha\to\gamma}\left(\mathbf{D}_0^{\gamma\to\alpha}\right)^{-1}\mathbf{T}_0^{\gamma\to\alpha} \quad (32)$$

The correspondence matrix $\mathbf{C}_0^{\gamma\to\alpha}$ can be calculated from equation (31) thanks to equation (8) and the coordinate transformation matrix reported in Table 1. It is

$$\mathbf{C}_0^{\gamma\to\alpha} = \mathbf{T}_0^{\gamma\to\alpha}\mathbf{D}_0^{\alpha\to\gamma} = \frac{1}{2}\begin{bmatrix} 0 & 2 & 0 \\ 1 & 0 & 1 \\ 1 & 0 & -1 \end{bmatrix} \quad (33)$$

It can be checked by using $\mathbf{T}_0^{\gamma\to\alpha}$ (Table 1) that the vector $[\bar{1}10]_\alpha$ in the parent crystal is at the place of the 2/3 $[1\bar{1}\bar{1}]_\gamma$ vector in the reference basis of the fcc crystal, which does not mean that the distortion preserves the parallelism of this direction. Indeed, it can be checked by using $\mathbf{C}_0^{\gamma\to\alpha}$ that the vector $[\bar{1}10]_\alpha$ is actually transformed into ½ $[2\bar{1}\bar{1}]_\gamma$. It can also be checked by using $\left(\mathbf{C}_0^{\gamma\to\alpha}\right)^*$ that the $(\bar{1}10)_\alpha$ plane once distorted becomes the $(1\bar{1}\bar{1})_\gamma$ plane of the fcc crystal.

5.2. Matrix of continuous lattice distortion

The continuous matrix of the bcc→fcc transformation can be calculated from the fcc→bcc matrix $\mathbf{D}_0^{\gamma\to\alpha}(\beta)$ given in ref. [2]. Let us recall that $\mathbf{D}_0^{\gamma\to\alpha}(\beta)$ is a function of the distortion angle β which varies from 60° to 70.5° during the fcc to bcc distortion. $\mathbf{D}_0^{\gamma\to\alpha}(60°)$ is the identity matrix; it lets the $\mathbf{B}_0^{\gamma}$ unchanged. $\mathbf{D}_0^{\gamma\to\alpha}(70.5°)$ is the complete transformation matrix; it transforms $\mathbf{B}_0^{\gamma}$ into $\mathbf{B}_0^{\gamma'}$ a basis of the bcc structure expressed into $\mathbf{B}_0^{\gamma}$; it is important to notice that $\mathbf{B}_0^{\gamma'}$ is not $\mathbf{B}_0^{\alpha}$. Actually $\mathbf{B}_0^{\gamma'}$ is constituted of the vectors $[001]_\alpha$, $[110]_\alpha$ and $[\bar{1}10]_\alpha$. Therefore, the bcc→fcc distortion matrix $\mathbf{D}_0^{\alpha\to\gamma}(\beta)$ is not simply the inverse of the fcc→bcc distortion matrix $\mathbf{D}_0^{\gamma\to\alpha}(\beta)$; one has also to calculate it in the reference basis of $\mathbf{B}_0^{\alpha}$. For that aim, let us split the fcc→bcc path into two successive paths: the first one from $\mathbf{B}_0^{\gamma}$ to $\mathbf{B}_0^{\gamma}$(β), and the next one from $\mathbf{B}_0^{\gamma}$(β) to $\mathbf{B}_0^{\gamma'}$. This decomposition, expressed in $\mathbf{B}_0^{\gamma}$, takes the form:

$$\mathbf{D}_0^{\gamma\to\alpha}(70.5°) = \left[\mathbf{B}_0^{\gamma} \to \mathbf{B}_0^{\gamma}(\beta)\right]\left[\mathbf{B}_0^{\gamma}(\beta) \to \mathbf{B}_0^{\gamma}(70.5°)\right] = \mathbf{D}_0^{\gamma\to\alpha}(\beta)\,(\mathbf{D}_0^{\alpha\to\gamma}(\beta))^{-1} \quad (34)$$

The last path is indeed the inverse of the path from the basis $\mathbf{B}_0^{\gamma'}$, which is a bcc basis, to the intermediate basis, both expressed in $\mathbf{B}_0^{\gamma}$; thus, it is the inverse of the bcc→fcc distortion matrix expressed $\mathbf{B}_0^{\gamma}$. Since the term "0" is not sufficient to avoid any confusion in the reference basis of the matrices $\mathbf{B}_0^{\gamma}$ or $\mathbf{B}_0^{\alpha}$, we wrote $\mathbf{D}_{/\gamma 0}^{\alpha\to\gamma}(\beta)$ in order to specify that the bcc→fcc distortion matrix $\mathbf{D}_{/\gamma 0}^{\alpha\to\gamma}(\beta)$ in equation (34) is written in $\mathbf{B}_0^{\gamma}$. From equation (34), it follows that

$$\mathbf{D}_{/\gamma 0}^{\alpha\to\gamma}(\beta) = \left(\mathbf{D}_0^{\gamma\to\alpha}\right)^{-1}\mathbf{D}_{/\gamma 0}^{\gamma\to\alpha}(\beta) \tag{35}$$

The two terms at the right of this equation are known from ref.[2]. They are the inverse of the matrix of complete transformation and the matrix of transformation at intermediate state given by the angle β. Eventually, the bcc→fcc transformation matrix $\mathbf{D}_{/\gamma 0}^{\alpha\to\gamma}(\beta)$ can be expressed in the reference basis $\mathbf{B}_0^{\alpha}$ by using the coordinate transformation matrix $\mathbf{T}_0^{\alpha\to\gamma} = \left[\mathbf{B}_0^{\alpha} \to \mathbf{B}_0^{\gamma}\right]$ given in Table 1. It becomes:

$$\mathbf{D}_0^{\alpha\to\gamma}(\beta) = \mathbf{D}_{/\alpha 0}^{\alpha\to\gamma}(\beta) = \mathbf{T}_0^{\alpha\to\gamma}\ \mathbf{D}_{/\gamma 0}^{\alpha\to\gamma}(\beta)\ \mathbf{T}_0^{\gamma\to\alpha} \tag{36}$$

The symbolic calculations, performed with Mathematica, lead to the components $d_{ij}^{\alpha\to\gamma}(\beta)$ of the matrix $\mathbf{D}_0^{\alpha\to\gamma}(\beta)$ expressed as function of X = cos(β):

(37)

$$d_{11}^{\alpha\to\gamma} = \frac{1}{72}(48 - 4\sqrt{6} + 9(-1 + 3\sqrt{6})\sqrt{X}\sqrt{\frac{1-X}{1+X}} + (11\sqrt{3} + 12\sqrt{2})\sqrt{1-X^2} + X(-48 + 8\sqrt{6} - (27\sqrt{3} + 9\sqrt{2})\sqrt{\frac{1-X}{1+X}}))$$

$$d_{12}^{\alpha\to\gamma} = \frac{1}{72}(-4\sqrt{6} + 9(1 - 3\sqrt{6})\sqrt{X}\sqrt{\frac{1-X}{1+X}} + (-7\sqrt{3} + 6\sqrt{2})\sqrt{1-X^2} + X(48 + 8\sqrt{6} + (27\sqrt{3} + 9\sqrt{2})\sqrt{\frac{1-X}{1+X}}))$$

$$d_{13}^{\alpha\to\gamma} = \frac{1}{36}(12 + 4\sqrt{6} - 8\sqrt{6}X - (2\sqrt{3} + 9\sqrt{2})\sqrt{1-X^2})$$

$$d_{21}^{\alpha\to\gamma} = \frac{1}{72}(48 - 4\sqrt{6} - 9(1 + 5\sqrt{6})\sqrt{X}\sqrt{\frac{1-X}{1+X}} + (11\sqrt{3} + 12\sqrt{2})\sqrt{1-X^2} + X(-48 + 8\sqrt{6} - (27\sqrt{3} + 9\sqrt{2})\sqrt{\frac{1-X}{1+X}}))$$

$$d_{22}^{\alpha\to\gamma} = \frac{1}{72}(-4\sqrt{6} + 9(1 + 5\sqrt{6})\sqrt{X}\sqrt{\frac{1-X}{1+X}} + (-7\sqrt{3} + 6\sqrt{2})\sqrt{1-X^2} + X(48 + 8\sqrt{6} + (27\sqrt{3} + 9\sqrt{2})\sqrt{\frac{1-X}{1+X}}))$$

$$d_{23}^{\alpha\to\gamma} = \frac{1}{36}(12 + 4\sqrt{6} - 8\sqrt{6}X - (2\sqrt{3} + 9\sqrt{2})\sqrt{1-X^2})$$

$$d_{31}^{\alpha\to\gamma} = \frac{1}{72}(48 - 4\sqrt{6} - 9(-2 + \sqrt{6})\sqrt{X}\sqrt{\frac{1-X}{1+X}} - (16\sqrt{3} + 15\sqrt{2})\sqrt{1-X^2} + X(-48 + 8\sqrt{6} + (54\sqrt{3} - 9\sqrt{2})\sqrt{\frac{1-X}{1+X}}))$$

$$d_{32}^{\alpha\to\gamma} = \frac{1}{72}(-4\sqrt{6} + 9(-2+\sqrt{6})\sqrt{X}\sqrt{\frac{1-X}{1+X}} + (20\sqrt{3} - 21\sqrt{2})\sqrt{1-X^2} + X(48 + 8\sqrt{6} - (54\sqrt{3} - 9\sqrt{2})\sqrt{\frac{1-X}{1+X}}))$$

$$d_{33}^{\alpha\to\gamma} = \frac{1}{18}(6 + 2\sqrt{6} - 4\sqrt{6}X - (\sqrt{3} - 9\sqrt{2})\sqrt{1-X^2})$$

This matrix is a function of the distortion angle β which varies from β = 70.5° (X = 1/3) to β = 60° (X=1/2) during the bcc to fcc distortion. One can check that $\mathbf{D}_0^{\alpha\to\gamma}(70.5°)$ is the identity matrix, and that the complete transformation $\mathbf{D}_0^{\alpha\to\gamma} = \mathbf{D}_0^{\alpha\to\gamma}(60°)$ is the matrix given in equation (31).

All the atoms M of the crystal are displaced during the bcc→fcc transformation exactly as those of the lattice:

$$\mathbf{PM'} = \mathbf{D}_0^{\alpha\to\gamma}(\beta)\,\mathbf{PM} \qquad (38)$$

The bcc→fcc transformation does not require shuffle.

5.3. Prediction of the habit plane

The complete transformation matrix $\mathbf{D}_0^{\alpha\to\gamma}$ in equation (31) gives the images of the directions by the bcc→fcc distortion in the reference basis $\mathbf{B}_0^{\alpha}$. The images of the planes are given by the inverse of its transpose:

$$(\mathbf{D}_0^{\alpha\to\gamma})^* = (\mathbf{D}_0^{\alpha\to\gamma})^{-T} = \begin{bmatrix} 1+\frac{\sqrt{6}}{18} & \frac{\sqrt{6}}{18} & \frac{1}{3}-\frac{\sqrt{6}}{6} \\ -\frac{1}{3}+\frac{\sqrt{6}}{18} & \frac{2}{3}+\frac{\sqrt{6}}{18} & \frac{1}{3}-\frac{\sqrt{6}}{6} \\ \frac{1}{3}-\frac{\sqrt{6}}{9} & \frac{1}{3}-\frac{\sqrt{6}}{9} & \frac{1}{3}+\frac{\sqrt{6}}{3} \end{bmatrix} \qquad (39)$$

The two matrices $\mathbf{D}_0^{\alpha\to\gamma}$ and $(\mathbf{D}_0^{\alpha\to\gamma})^*$ give in the initial basis $\mathbf{B}_0^{\alpha}$ the images of the directions and planes, respectively. These images are directly expressed in the final base $\mathbf{B}_0^{\gamma}$ by using the correspondence matrices $\mathbf{C}_0^{\gamma\to\alpha}$ of equation (33) and $(\mathbf{C}_0^{\gamma\to\alpha})^*$, respectively. The results obtained on the low-index directions and planes are reported in Table 2. This table can be compared with the one given for the fcc→bcc transformation (Table 1 of ref. [2]). It can be noticed that the results are identical if the directions and planes are exchanged.

As in ref. [2], the HP is determined as the plane **g** untilted by the distortion. The rotation amplitude of a plane **g** (normalized reciprocal vector) is given in Fig. 7 as a function of the spherical coordinate angles θ and ϕ of **g**. As for fcc→bcc transformation [2], four solutions are found; they can be grouped into two pairs due to the fact that the solutions at θ > π/2 are equivalent to those obtained at θ ≤ π/2 because of the centrosymmetric equivalence (θ, ϕ) ≡ (π-θ, ϕ+π). Thus, there are two non-equivalent solutions, one at $(\theta = 1.571, \phi = 2.356)$ which corresponds to the $(\bar{1}10)_\alpha$ plane, and the other one at $(\theta = 1.222, \phi =$

$2.616)$ which corresponds to the plane $(-0.813, 0.471, 0.341)_\alpha$. The exact value, calculated from the eigenvectors of the reciprocal distortion matrix $\left(\mathbf{D}_0^{\alpha\to\gamma}\right)^*$ is $(-7-2\sqrt{6},\ 2+2\sqrt{6},\ 5)_\alpha$ plane which is at 1.3° of the rational plane $(\bar{5}32)_\alpha$. It can be checked that it is exactly the image of the HP predicted analytically for the fcc→bcc transformation. Actually, the fact that the HP of the bcc→fcc transformation is the same as for the bcc→fcc transformation is a logical consequence of the criterion (10): since in our analysis, the HP is assumed to be an untilted plane; this plane is the same for both direct and inverse transformations.

There are few experimental studies on the HPs in pure bcc→fcc transformations. Ohmori *et al.* [31] report that the Widmanstätten austenite γ laths are in KS OR with the ferritic δ matrix and exhibit a well-defined $(\bar{1}10)_\delta$ // $(\bar{1}11)_\gamma$ HP with the growth direction parallel to $[111]_\delta$ // $[110]_\gamma$, which is completely coherent with the first solution found for $(\theta = 1.571, \phi = 2.356)$. The same OR and the same HP were observed for the bcc→fcc transformation obtained by heating martensitic steels to produce reverse austenite [28][29]. In Cu-Zn brass, Srinivasan and Hepworth [35] investigated the HPs by Laue diffraction and reported two possible different HPs indexed in the parent α bcc phase: $(2, 11, 12)_\alpha$ and $(123)_\alpha$ with a large scatter of the results depending on the alloy composition; but interestingly the scatter is not random and actually the HPs are aligned in the pole figure on a segment containing the $<111>_\alpha$ dense direction and located between the two extreme $(2, 11, 12)_\alpha$ and $(123)_\alpha$ planes (Fig. 3 of ref. [35]). Unfortunately, the authors did not precise the corresponding OR without the ambiguities of the parent symmetries, which impedes a direct comparison with our calculations. We can just notice here that the $(\overline{12}, 11, 2)_\alpha$ plane is at 7.4° from the calculated $(\bar{1}10)_\alpha$ HP, the $(\bar{3}21)_\alpha$ HP is at 4.3° from the calculated $(\bar{5}32)_\alpha$ HP, and the common $<111>_\alpha$ dense direction is in good agreement with the neutral line chosen for our calculations. It could be worth studying more in details the HPs in Cu-Zn alloys to get more precise and statistical experimental results for comparison. It should be also acknowledged that the assumptions taken in our calculations are probably too rudimentary: the atoms in Cu-Zn alloys do not have the same size, which means that the hard-sphere model with a unique size is not appropriate, and the daughter phase is not perfectly fcc, but orthorhombic or monoclinic 9R.

6. BCC→HCP transformations

6.1. Matrix of complete lattice distortion

As for fcc→hcp transformation, since the primitive unit cell of the hcp phase contains two atoms, it is not possible to find a homogenous distortion that transforms a bcc crystal into a hcp crystal, and thus a shuffle is required for half of the atoms in the lattice. By considering Fig. 5 and Fig. 6b, it appears that the vectors **PO** =½ $[111]_\alpha$ and **PN** = $[\bar{1}10]_\alpha$ remain invariant during the transformation, and that only vector **PK** =½ $[11\bar{1}]_\alpha$ is rotated such that the angle (**P0**,**PK**) which is initially 70.5° decreases to 60°. The natural choice of the primitive basis $\mathbf{B}_p^\alpha$ is therefore **x** = **PO** =½ $[111]_\alpha$, **y** = **PK** =½ $[11\bar{1}]_\alpha$ and **z** = **PN** = $[\bar{1}10]_\alpha$. They are transformed into the vectors **PO** = $[100]_\varepsilon$, **PK** = $[110]_\varepsilon$ and **PN** = $[001]_\varepsilon$ respectively, as illustrated in Fig. 5 .

This means that $\mathbf{B}_p^{\alpha} = \begin{bmatrix} 1/2 & 1/2 & -1 \\ 1/2 & 1/2 & 1 \\ 1/2 & -1/2 & 0 \end{bmatrix}$ expressed in the basis $\mathbf{B}_0^{\alpha}$, has for image in the basis of the product phase $\mathbf{B}_0^{\varepsilon}$, the basis $\mathbf{B}_{p\,/\varepsilon 0}^{\alpha'} = \begin{bmatrix} 1 & 1 & 0 \\ 0 & 1 & 0 \\ 0 & 0 & 1 \end{bmatrix}$.

This image can be calculated in the reference basis of the parent crystal $\mathbf{B}_0^{\alpha}$ by using the coordinate transformation matrix $\mathbf{T}_0^{\alpha\to\varepsilon} = [\mathbf{B}_0^{\alpha} \to \mathbf{B}_0^{\varepsilon}]$ given in Table 1. It follows that $\mathbf{B}_p^{\alpha'} = \mathbf{T}_0^{\alpha\to\varepsilon}\,\mathbf{B}_{p\,/\varepsilon 0}^{\alpha'}$ and then $\mathbf{D}_0^{\alpha\to\varepsilon} = \mathbf{T}_0^{\alpha\to\varepsilon}\,\mathbf{B}_{p\,/\varepsilon 0}^{\alpha'}\left(\mathbf{B}_p^{\alpha}\right)^{-1}$, which becomes after calculations

$$\mathbf{D}_0^{\alpha\to\varepsilon} = \begin{bmatrix} \frac{1}{16}(14+\sqrt{6}) & \frac{1}{16}(-2+\sqrt{6}) & \frac{1}{8}(2-\sqrt{6}) \\ \frac{1}{16}(-2+\sqrt{6}) & \frac{1}{16}(14+\sqrt{6}) & \frac{1}{8}(2-\sqrt{6}) \\ \frac{1}{8}(3-\sqrt{6}) & \frac{1}{8}(3-\sqrt{6}) & \frac{1}{4}(1+\sqrt{6}) \end{bmatrix} \qquad (40)$$

The correspondence matrix $\mathbf{C}_0^{\varepsilon\to\alpha}$ is then calculated thanks to equation (8) and the coordinate transformation matrix reported in Table 1. It is

$$\mathbf{C}_0^{\varepsilon\to\alpha} = \mathbf{T}_0^{\varepsilon\to\alpha}\mathbf{D}_0^{\alpha\to\varepsilon} = \frac{1}{2}\begin{bmatrix} 2 & 2 & 0 \\ 1 & 1 & -2 \\ -1 & 1 & 0 \end{bmatrix} \qquad (41)$$

It can be checked by using $\mathbf{T}_0^{\varepsilon\to\alpha}$ (Table 1) that the vector $[\bar{1}10]_\alpha$ in the parent crystal is at the place of the [001] vector in the reference basis of the hcp crystal. It can be checked by using $\mathbf{C}_0^{\varepsilon\to\alpha}$ that the vector $[\bar{1}10]_\alpha$ is also transformed into [001] , and by using $(\mathbf{C}_0^{\varepsilon\to\alpha})^*$ that the $(\bar{1}10)_\alpha$ plane once distorted becomes the $(002)_\varepsilon$ plane of the hcp crystal.

6.2. Matrix of continuous transformation

The distortion matrix of the bcc→hcp transformation can be calculated with the method used for the fcc→bcc transformation [2]. Let us consider the non-orthogonal frame $\mathbf{B}_p^{\alpha}$ constituted by the normalized axes **x** = $(1/\sqrt{3})[111]_\alpha$, **y** = $(1/\sqrt{3})[11\bar{1}]_\alpha$, and **z** = $(1/\sqrt{2})[\bar{1}10]_\alpha$, as illustrated in Fig. 5. The $[111]_\alpha$ and $[11\bar{1}]_\alpha$ directions define the $(\bar{1}10)_\alpha$ plane that is transformed into the basal $(001)_\varepsilon$ plane by the distortion. Now, let us associate the orthonormal basis $\mathbf{B}_s^{\alpha}$ = ($\mathbf{x}_s$, $\mathbf{y}_s$, $\mathbf{z}_s$) with the basis $\mathbf{B}_p^{\alpha}$ = (**x**, **y**, **z**) as in ref. [2] and as usually done for the structural tensor, i.e., $\mathbf{x}_s$ // **x**, $\mathbf{y}_s \in$ (**x**, **y**) and $\mathbf{y}_s \perp$ **x**, $\mathbf{z}_s \perp$ **x**, $\mathbf{z}_s \perp$ **y** and $\mathbf{z}_s$ points in the same direction as **z**. The coordinates of the **x**, **y** and **z** vectors in the basis $\mathbf{B}_s^{\alpha}$ give the coordinate transformation matrix from $\mathbf{B}_s^{\alpha}$ to $\mathbf{B}_p^{\alpha}$, which is function of the angle β:

$$\left[\mathbf{B}_s^{\alpha} \rightarrow \mathbf{B}_p^{\alpha}(\beta)\right] = \begin{bmatrix} 1 & \cos(\beta) & 0 \\ 0 & \sin(\beta) & 0 \\ 0 & 0 & 1 \end{bmatrix} \quad (42)$$

The distortion matrix can be expressed in the basis $\mathbf{B}_p^{\alpha}$ by

$$\mathbf{D}_p^{\alpha\rightarrow\varepsilon}(\beta) = \left[\mathbf{B}_p^{\alpha}(70.5°) \rightarrow \mathbf{B}_p^{\alpha}(\beta)\right] = \left[\mathbf{B}_p^{\alpha}(70.5°) \rightarrow \mathbf{B}_s^{\alpha}\right]\left[\mathbf{B}_s^{\alpha} \rightarrow \mathbf{B}_p^{\alpha}(\beta)\right] \quad (43)$$

This matrix can be expressed in the reference basis $\mathbf{B}_0^{\alpha}$ by

$$\mathbf{D}_0^{\alpha\rightarrow\varepsilon}(\beta) = \left[\mathbf{B}_0^{\alpha} \rightarrow \mathbf{B}_p^{\alpha}(70.5°)\right] \mathbf{D}_p^{\alpha\rightarrow\varepsilon}(\beta) \left[\mathbf{B}_0^{\alpha} \rightarrow \mathbf{B}_p^{\alpha}(70.5°)\right]^{-1} \quad (44)$$

which becomes after calculations

$$\mathbf{D}_0^{\alpha\rightarrow\varepsilon}(\beta) = \frac{1}{4}\begin{bmatrix} 3+X+\frac{\sqrt{1-X^2}}{\sqrt{2}} & -1+X+\frac{\sqrt{1-X^2}}{\sqrt{2}} & 2-2X-\sqrt{2}\sqrt{1-X^2} \\ -1+X+\frac{\sqrt{1-X^2}}{\sqrt{2}} & 3+X+\frac{\sqrt{1-X^2}}{\sqrt{2}} & 2-2X-\sqrt{2}\sqrt{1-X^2} \\ 1+X-\sqrt{2}\sqrt{1-X^2} & 1+X-\sqrt{2}\sqrt{1-X^2} & 2-2X+2\sqrt{2}\sqrt{1-X^2} \end{bmatrix} \quad (45)$$

with X = cos(β).

One can check that for the initial state, since β = 70.5° (X = 1/3), $\mathbf{D}_0^{\alpha\rightarrow\varepsilon}(70.5°)$ is the identity matrix, and that the complete transformation obtained for β = 60° (X = 1/2) is the matrix (40).

6.3. Schuffle

All the atoms of type N = (*u*, *v*, *w*) located as N in the plane $(\bar{1}10)_\alpha$ of even layers, i.e. such that *l = (-u+v)* is even, have a trajectory that follows directly the lattice distortion:

$$\mathbf{PN'} = \mathbf{D}_0^{\alpha\rightarrow\varepsilon}(\beta)\,\mathbf{PN} \quad (46)$$

All the other atoms of type M = (*u*, *v*, *w*) located as M in the plane $(\bar{1}10)_\alpha$ of odd layers, i.e., such that *l = (-u+v)* is odd, have a trajectory that does not follow directly the lattice distortion, but that can be deduced of it. They describe locally in their cells the same trajectory as for the bcc→fcc transformation $\mathbf{D}_0^{\alpha\rightarrow\gamma}(\beta)$, as illustrated in Fig. 6a and Fig. 6b. Two shuffle directions are possible: one in which M moves towards P, and one in which it moves in the opposite direction towards R (Fig. 5c). The origin P of the unit cell in which the atom M is located is deduced from M by the translation vector **t** = $[010]_\alpha$. Thus, the two possible shuffles of M, noted S1 and S-1, are given by

Shuffle S1: $\mathbf{PM'} = \mathbf{D}_0^{\alpha\rightarrow\varepsilon}(\beta)\,(\mathbf{PM}-\mathbf{t}) + \mathbf{D}_0^{\alpha\rightarrow\gamma}(\beta)\,\mathbf{t}$, with **t** = ½ $[010]_\alpha$ (47)

Shuffle S-1: $\mathbf{PM'} = \mathbf{D}_0^{\alpha\rightarrow\varepsilon}(\beta)\,(\mathbf{PM}-\mathbf{t}) - \mathbf{D}_0^{\alpha\rightarrow\gamma}(\beta)\,\mathbf{t}$, with **t** = ½ $[010]_\alpha$ (48)

Therefore, contrarily to the bcc→fcc transformation, but as for the fcc→hcp transformation, the

bcc→hcp transformation requires a shuffle of half of the atoms in the lattice. The two equivalent shuffles were already noticed by Burgers in his early work [4], even if not analytically expressed as here. They are at the origin of the stacking faults in the hcp laths observed by TEM in titanium alloys [38].

6.4. Habit plane

The matrix (40) gives the images of the directions by the bcc→hcp distortion in the reference basis $\mathbf{B}_0^{\alpha}$. The images of the planes are given by the inverse of its transpose:

$$(\mathbf{D}_0^{\alpha\to\varepsilon})^* = (\mathbf{D}_0^{\alpha\to\varepsilon})^{-T} = \frac{1}{18}\begin{bmatrix} 15+\sqrt{6} & -3+\sqrt{6} & 6-3\sqrt{6} \\ -3+\sqrt{6} & 15+\sqrt{6} & 6-3\sqrt{6} \\ 6-2\sqrt{6} & 6-2\sqrt{6} & 6(1+\sqrt{6}) \end{bmatrix} \qquad (49)$$

The two matrices $\mathbf{D}_0^{\alpha\to\varepsilon}$ and $(\mathbf{D}_0^{\alpha\to\varepsilon})^*$ give in the initial basis $\mathbf{B}_0^{\alpha}$ the images of the directions and planes , respectively. These images can be calculated in the final base $\mathbf{B}_0^{\varepsilon}$ by using the correspondence matrices $\mathbf{C}_0^{\alpha\to\varepsilon}$ given by equation (41) and $(\mathbf{C}_0^{\alpha\to\varepsilon})^*$, respectively. The images of the low-index directions and planes are given in Table 3.

As in previous sections, it is also possible to determine the HP as the plane untilted by the distortion. The rotation amplitude is given as a function of the spherical coordinate angles θ and ϕ in Fig. 8. Here six solutions are found. They can be grouped into two triplets due to the fact that the solutions at $\theta > \pi/2$ are equivalent to those obtained at $\theta \leq \pi/2$ because of the centrosymmetric equivalence of lines $(\theta, \phi) \equiv (\pi-\theta, \phi+\pi)$. Thus, there are three unequivalent solutions. The exact values calculated by the eigenvectors of the reciprocal distortion matrix are $(\bar{1}\bar{1}2)_\alpha$, $(\bar{1}10)_\alpha$ and $(-\sqrt{6},-\sqrt{6},2)_\alpha$. This last plane is at 0.5° of the rational plane $(\bar{5}\bar{5}4)_\alpha$; and it is transformed into $(\sqrt{6}-1,2,0)_\varepsilon \approx (340)_\varepsilon$ by the distortion. Actually the solutions $(\bar{1}10)_\alpha$ and $(-\sqrt{6},-\sqrt{6},\ 2)_\alpha$ are associated with the same eigenvalue 1, which means that they form a 2D vector space, and any linear combination of these two vectors should be also an eigenvector. However, for a reason that is not completely clear to us, any approximation on any of nine irrational component of the distortion matrix makes the 2D space condensates into the two vectors $(\bar{1}10)_\alpha$ and $(-\sqrt{6},-\sqrt{6},2)_\alpha$. Contrarily to all the phase transformations described in the previous sections, the plane of the third solution $(-\sqrt{6},-\sqrt{6},2)_\alpha$ does not contain the neutral line.

There are a lot of scatter in the HPs reported in titanium and zirconium alloy, but many studies report the $\{443\}_\alpha$ HP (it is recalled again that α is the bcc phase in our study). Although a direct comparison is difficult because of the symmetries of the parent bcc phase, it can be noticed that the calculated $(\bar{5}\bar{5}4)_\alpha$ plane is at 1.5° from the $(\bar{4}\bar{4}3)_\alpha$ HP. However, such good matching could be a coincidence. Indeed, other HPs have been reported for which the agreement is not as good. In a recent paper, Qiu *et al.* [48] deeply investigated by TEM the martensitic plates in a Ti-Cr alloy and they indexed unambiguously all their diffraction patterns according a particular Burgers OR chosen among the equivalent ones. The HP of the “type M plate” they investigated, written with our choice of Burgers OR, is $(\bar{4}\bar{4}5)_\alpha$ // $(130)_\varepsilon$. Our calculated $(\bar{5}\bar{5}4)_\alpha$ // $(340)_\varepsilon$ HP is at the 12° far from their reported $(\bar{4}\bar{4}5)_\alpha$ // $(130)_\varepsilon$ HP. This agreement is qualitatively quite good because

both calculated and reported HPs are perpendicular to the hcp basal plane, but not quantitatively sufficient for the moment to compete with the PTMC [42][43] or E2EM [44][48] models. The quantitative discrepancy could be due to the fact that in real alloys the hard-sphere approximation is not sufficiently accurate anymore because of the difference of size of the Ti atoms in the bcc and hcp phases, the real $c_\varepsilon/a_\varepsilon$ ratio different from the ideal one, and because the transformation occurs in an alloy and not in a mono-atomic phase.

The continuous analytical expressions of the angular distortive matrices of bcc→fcc and bcc→hcp transformations have been represented with VPython. Simulation "movies" of the distortion of a bcc cube constituted by 6x6x6 unit cells transformed into fcc and hcp structure are given in Supplementary Materials S5 and S6, respectively. The initial, intermediate and final states are represented in blue, yellow and red colors, respectively, in Fig. 9a and b.

7. Discussion

7.1. Vocabulary and associated concepts

Before starting the discussion, and in order to avoid any misunderstanding that could be source of controversy, we think it is important to precise the concept behind some words. The term "transition" is used more generally by physicists, and "transformation" by metallurgists; the former treats the cases of phase change with no or only short-range order rearrangements of the atoms, whereas the latter also includes long range diffusion and therefore precipitation. The term "displacive" was initially attributed to transformations involving collective displacements of atoms, which is inevitably correlated to the distortion of the lattice. In the paper, we use equivalently "transition", "displacive transformation" and "martensitic transformation". The term "reconstructive" needs clarification because it may lead to important confusions, as already noticed by Otsuka and Ren in their review paper on Ti-Ni shape memory alloys [49]. In crystallography, "reconstructive" means that some of the atomic bounds in the parent phase are broken and new bounds are formed in the daughter phase; some symmetry elements of the parent phase are lost and new ones are "reconstructed" in the daughter phase [50]. In metallurgy, the term "reconstructive" is synonymous of "diffusive", and thus includes long range ordering or precipitation mechanisms, and is often used in opposition to the term "displacive". All the fcc-hcp-bcc transformations treated in the present paper are classified as both "reconstructive" and "displacive" in crystallography, but only as "displacive" in metallurgy. In the rest of the discussion the term "reconstructive" will be used with its crystallographic meaning.

In metallurgy, the formation of a relief at a polished surface is often associated with displacive transformations but not exclusively; and this has split the community of metallurgists into two groups: the "shearists" and the "diffusionists" [51]. To briefly summarize, the "shearists" assume that a surface relief can be created only by a displacive mechanism [52][53] whereas the "diffusionists" think that in some alloys it is created by diffusion, with the formation of "terraces of growth ledges" with an atomic correspondence at the parent/daughter interface [57][58]. Both groups have developed their own crystallographic tools to predict the orientation relationships and habit planes; i.e., the PTMC for the

former, and the E2EM or equivalent for the latter [51]. The “diffusionists” often use the term “precipitation” in their studies on lath or plate formation in the fcc-hcp-bcc system. However, the term “precipitation” will be considered in the present paper in a very strict meaning, such as it is in aluminum alloys [59]. Some atoms of specie Y that are in solid solution in a matrix constituted of atoms of specie X, diffuse and migrate due to their chemical driving forces; first, they make small clusters which then grow slowly each time a new atom Y joins the cluster. The atoms Y, associated or not with the atoms X or to other species, form a new crystallographic structure which is in OR with the matrix in order to minimize the interfacial misfits. Sometimes a reordering of the atoms in the precipitate structure during the precipitation growth occurs due to a size effect [60]. During their growth the precipitates become semi-coherent, and incoherent at micron-scale. Since the atoms come from all around the surrounding cluster, the precipitation mechanism is isotropic, and the precipitate shape is only a consequence of the symmetries of the precipitate and matrix phases (see section 7.3). The precipitates are generally metastable and dissolve during thermal treatments at high temperatures, and the Y species re-precipitate to form new stable phases, such as Mg_2Si in 6xxx alloys. It is clear that the approach and equations described in the present paper do not apply to precipitation.

The term “twinning” has very broad meaning that comes from the early Friedel’s work on mineralogy; he states: “*A twin is a complex edifice built up of two or more homogeneous portions of the same crystal species in contact (juxtaposition) and oriented with respect to each other according to well-defined law*” [61](see also ref. [62]). It means that in a polycrystalline material any misorientation found with a frequency higher than it could be expected from a random distribution of isotopic orientations is a “twin”. This definition includes annealing twins, mechanical (micro- and macro-) twins, and it also comprises the specific misorientations that exist between the variants after a phase transformation, i.e., the transformation twins. However, to our point of view, annealing and mechanical twins are slightly different from transformation twins. In the former case a crystal γ_0 of phase γ is transformed into another crystal γ_1 of same phase, whereas in the latter case, a parent crystal γ_0 of phase γ is transformed into many distinct variants α_i of phase α, and the misorientation between two variants α_i can be understood only by considering their parent crystal. In the first versions of PTMC [54][55] the lattice invariant shears were mechanical twins (or dislocations) whereas in its advanced versions [56] it includes the “twin” boundaries between pairs of (self-accommodating) variants. Annealing and mechanical twins should also be distinguished: the former results from a diffusion process, as precipitation, whereas the latter results from a lattice distortion induced by stress. In the rest of the discussion, the term “twin” and “twinning” will only apply to mechanical twinning.

7.2. Angular distortive matrices for the transitions in the fcc-hcp-bcc Burgers triangle

The repetitive style of the paper was chosen on purpose. The aim was to show that the approach and mathematics are very similar for all the displacive transformations and mechanical twinning in the fcc-bcc-hcp system. Any transition or mechanical twinning can be represented by an angular distortive matrix with a unique order parameter which is the angle of distortion. It can be noted that the nine components of all the matrices of complete transitions between the three hard-sphere packed phases are a sum of a rational

number and rational number times $\sqrt{6}$; i.e. these matrices are built on an extension of the field of rational numbers $\mathbb{Q}$ by $\sqrt{6}$: they form an algebra over the field $\mathbb{Q}(\sqrt{6})$.

For mechanical twinning, the calculations have been performed only for fcc-fcc, but there is no obstacle to perform them for twinning in hcp or bcc metals. For example, we have calculated the distortion matrix associated with the recently reported "anomalous" $\{10\bar{1}2\}$ mechanical twinning in magnesium [63], and are able to explain their formation despite their apparent negative Schmidt factors. The details will be presented in a next paper [64].

The distortion matrices can be used to determine the HPs numerically and analytically assuming that they correspond to untilted planes, i.e. they are among the eigenvectors of the reciprocal distortion matrix. Thus, in general, the maximum number of possible HPs for one distortion matrix is three. The only exception occurs when two eigenvalues are equal, which means that their associated eigenvectors form a 2D vector space (if they are not parallel). This is the case for the bcc→hcp transition; however it was also noticed that the vector space is very instable, i.e. any approximation on the irrational values of the distortion matrix makes the 2D space disappear and replaced by two distinct and discrete vectors. In the case of three solutions, one can raise the question: what is the HP among them? For transitions in which the untilted plane is fully invariant, such as fcc-hcp transition or fcc-fcc twinning, the HP is the invariant plane. However, for the other transitions, the answer is less trivial. We noticed that in these cases the HP is often the irrational (high index) plane. One reason could be that the volume change is localized inside the angular distortion of the low index plane, such as the $(\bar{1}11)_\gamma \rightarrow (\bar{1}10)_\alpha$ distortion of the fcc→bcc martensitic transformation, which means that the deformation in this plane can't be accommodated, whereas the untilted irrational plane can be transformed into a fully invariant plane by variant grouping, as we have shown for the $\{225\}_\gamma$ HPs of martensitic steels [3]. However, such considerations still lack generality and further work is required to establish a rigorous law that determines the correct HP in the set of the eigenvectors of reciprocal distortion matrix.

In addition to the determination of the HPs, the distortion matrices calculated in the paper could be useful to estimate the strain field in the surrounding matrix. They could pave the way for a new mechanics of deformation by phase transformation or mechanical twinning, a mechanics that would not involve shear, but tensor products between the stress and distortion matrices. The perspectives are very large and can't be detailed here. We will just introduce the concept of distortional variant that will be of prime importance for these researches and needs to be clarified and explained.

7.3. Orientational and distortional variants

The orientational variants are the distinct orientations of the daughter crystals formed by a phase transformation. The orientational variants depend only on the symmetries of the parent and daughter phases and on the OR; they do not depend on the transformation mechanism. The orientational variants can be the orientations of martensite laths in martensitic steels (displacive transformation) or the orientation of precipitates in aluminium alloys (diffusive transformation). Let us call $\mathfrak{G}^\gamma$ and $\mathfrak{G}^\alpha$ the point groups of the parent and daughter phases, respectively. The point groups are noted by capital bold letters

in Algerian font in the paper. They are sets of symmetry 3x3 matrices. Let us call also $\mathbf{T}_0^{\gamma\to\alpha}$ the coordinate transformation matrix deduced from the OR as shown in equation (3). The matrix $\mathbf{T}_0^{\gamma\to\alpha}$ results from the choice of equivalent planes and directions chosen to write this OR. It is calculated for one variant, arbitrarily chosen to be the variant 1, α_1. Thus $\mathbf{T}_0^{\gamma\to\alpha} = \mathbf{T}_0^{\gamma\to\alpha_1}$. For example the point group $\mathbf{G}^\gamma$ is the set of matrices expressed in the basis $\mathbf{B}_0^\gamma$ simply noted g_i^γ. The symmetries of the daughter crystal expressed in the basis $\mathbf{B}_0^\gamma$ are given by the set of matrices $\mathbf{T}_0^{\gamma\to\alpha}\,\mathbf{G}^\gamma\,(\mathbf{T}_0^{\gamma\to\alpha})^{-1}$. The intersection group is the group of the symmetries that are common to both the parent crystal and the daughter crystal α_1 ; it is

$$\mathbf{H}^\gamma = \mathbf{G}^\gamma \cap \mathbf{T}_0^{\gamma\to\alpha}\,\mathbf{G}^\alpha\,(\mathbf{T}_0^{\gamma\to\alpha})^{-1} \tag{50}$$

The set $\mathbf{H}^\gamma$ is a subgroup of $\mathbf{G}^\gamma$, i.e. $\mathbf{H}^\gamma \leq \mathbf{G}^\gamma$. The distinct orientational variants α_i are defined by the cosets $\alpha_i = g_i^\gamma \mathbf{H}^\gamma$ and their orientations by

$$\mathbf{T}_0^{\gamma\to\alpha_i} = \left[\mathbf{B}_0^\gamma \to \mathbf{B}_0^{\alpha_i}\right] = g_i^\gamma \mathbf{T}_0^{\gamma\to\alpha} \text{ with } g_i^\gamma \in \alpha_i \tag{51}$$

One must understand " $g_i^\gamma \in \alpha_i$ ", as g_i^γ arbitrarily chosen in the coset α_i. By convention, g_1^γ is the identity matrix. The number of orientational variants N^α is the number of cosets on $\mathbf{H}^\gamma$; i.e. the cardinal of $\mathbf{G}^\gamma/\mathbf{H}^\gamma$ and is given by the Lagrange formula: $N^\alpha = |\mathbf{G}^\gamma|/|\mathbf{H}^\gamma|$. For precipitates (diffusive transformation), the symmetries of their shape are also given by $\mathbf{H}^\gamma$. More details on the orientational variants can be found in [65] [66].

Contrarily to precipitates, the shape of the martensite products (needle, lath, plates, lenticular shapes) does not depend on $\mathbf{H}^\gamma$, but on the symmetries of the parent phase that are preserved by the distortion mechanism. Let us consider a parent crystal of shape with symmetries given by $\mathbf{G}^\gamma$. The crystal after complete distortion, i.e. a crystal of daughter phase, has a shape with symmetries given by matrices expressed in the basis $\mathbf{B}_0^\gamma$ by $\mathbf{D}_0^{\gamma\to\alpha}\,\mathbf{G}^\gamma\,(\mathbf{D}_0^{\gamma\to\alpha})^{-1}$. The intersection group is the group of the symmetries that are common to both the crystal before and after distortion; it is

$$\mathbf{K}^\gamma = \mathbf{G}^\gamma \cap \mathbf{D}_0^{\gamma\to\alpha}\,\mathbf{G}^\gamma\,(\mathbf{D}_0^{\gamma\to\alpha})^{-1} \tag{52}$$

with $\mathbf{K}^\gamma \leq \mathbf{G}^\gamma$. The distinct distortional variants d_i are defined by the cosets $d_i = g_i^\gamma \mathbf{K}^\gamma$. Their number of variants M^α is the number of cosets on $\mathbf{K}^\gamma$; it is the cardinal of $\mathbf{G}^\gamma/\mathbf{K}^\gamma$ and is given by the Lagrange formula: $M^\alpha = |\mathbf{G}^\gamma|/|\mathbf{K}^\gamma|$.

The distortion matrix of the variant d_i is expressed locally in the basis $\mathbf{B}_i^\gamma$ by the matrix $\mathbf{D}_i^{\gamma\to\alpha_i} = \mathbf{D}_0^{\gamma\to\alpha}$. Thus, the distortion matrix of a variant d_i expressed in the basis $\mathbf{B}_0^\gamma$ is

$$\mathbf{D}_0^{\gamma\to\alpha_i} = \left[\mathbf{B}_0^\gamma \to \mathbf{B}_i^{\alpha_i}\right] \mathbf{D}_i^{\gamma\to\alpha_i} \left[\mathbf{B}_i^{\alpha_i} \to \mathbf{B}_0^\gamma\right] = g_i^\gamma\, \mathbf{D}_0^{\gamma\to\alpha} \left(g_i^\gamma\right)^{-1} \text{ with } g_i^\gamma \in d_i \tag{53}$$

The distortion matrices $\mathbf{D}_0^{\gamma\to\alpha_i}$ will be of prime importance to calculate the mean distortion generated by pair and set of variants. They will be used to show that it is possible to make the untilted $\{225\}_\gamma$ planes fully invariant [3].

Equations (50) and (52) show the difference between orientational and distortional variants. Generally, $\mathbf{K}^\gamma \leq \mathbf{H}^\gamma$ (the demonstration, not reported here, is based on equation (8)), which means that the number of distortional variants is higher than the number of orientational variants: $M^\alpha \geq N^\alpha$. Let us illustrate this difference in the case of the fcc→hcp transformations (Fig. 10). The intersection group of orientations $\mathbf{H}^\gamma$ contains 12 symmetries elements, thus $N^\alpha = 4$. There are four orientational variants. Moreover the shape of hcp precipitates in a fcc matrix has symmetries given by $\mathbf{H}^\gamma$. The 3-fold axis normal to the common dense plane $(\bar{1}11)_\gamma$ // $(001)_\varepsilon$ of the hcp precipitates is an element of $\mathbf{H}^\gamma$, which explains why the precipitates have a triangular shape. In the case of martensitic transformation, only one of the three equivalent $<112>_\gamma$ vector is the "shear" vector at the origin of the transformation, or equivalently in our approach, only one of the three equivalent **z** = **PN** should be chosen to be transformed into the $[001]_\varepsilon$ axis (Fig. 3c), and thus $\mathbf{H}^\gamma$ is broken by this "choice" into a subgroup $\mathbf{K}^\gamma < \mathbf{H}^\gamma$, and $\mathbf{K}^\gamma$ contains 4 elements. The hcp variants formed by distortion have a shape symmetries $\mathbf{K}^\gamma$, and not $\mathbf{H}^\gamma$, and thus are not triangular anymore. Actually, if martensite is created by cooling, the three "shear" modes can operate successively on layers of thickness around 50 nm to accommodate the distortion strains [67]. However, if the transformation is triggered by imposing a shear [68], only one variant will be activated so that the distortion strain accommodates the imposed shear. In the case of fcc→bcc martensitic transformation with KS OR, since $\mathbf{H}^\gamma$ only contains the identity and inversion elements, $\mathbf{H}^\gamma$ can't be broken by the distortion, and thus $\mathbf{K}^\gamma = \mathbf{H}^\gamma$. A brief summary of the algebraic formula used to calculate the orientational and distortional variants for direct and inverse transformations is given in Table 4.

7.4. Orientation gradients induced by distortion

The main idea in our approach is that the atoms move during the transformation as if they roll collectively on each other; and it is these movements which generate the lattice distortion. The mechanism operates whatever the plastic deformation modes of the parent matrix in which the daughter martensite forms. A good image is the solidification of water in a rigid bottle: if the undercooling is sufficiently high, the dilatation induced by the phase change breaks the bottle whatever its constituent material (actually, if the bottle can withstand internal pressures higher than 220 MPa, a new phase of ice denser than water will form). This concept is very basic but has many implications in our model of displacive transformations. For example, all the distortion matrices have been calculated independently of the exact plastic behavior of the matrix, contrarily to the PTMC approaches which includes the shear relaxation modes in the core of the theory. As already schematized in ref. [2], we think that the global accommodation in the matrix generated by arrays of accommodating dislocations is a direct consequence of the lattice distortion and not, in first approximation, of the details of the accommodation modes. Of course the exact nature of the dislocations (screw, edge, partial etc.) depends on the structure of the parent phase, but probably the global mesoscopic orientation gradients do not. An experimental observation that supports this point of view is

the fact that in the fcc-bcc system, the continuous features observed in the Electron BackScatter Diffraction (EBSD) pole figures of the variants belonging to the same parent grains are very similar for direct and inverse transformations, whatever the plastic deformation mode of the parent phase, fcc or bcc, i.e. gliding on the $\{111\}_\gamma$ planes for fcc, or on the $\{110\}_\alpha$ and $\{112\}_\alpha$ planes for bcc. This is illustrated in Fig. 11 which shows that the features of the bcc laths generated in a martensitic steels by the fcc→bcc transformation (Fig. 11a) are similar to those of the fcc Widmanstätten laths generated in a brass by the bcc→fcc transformation (Fig. 11b, from [36]), or to those of the fcc plates generated in duplex steels (Fig. 11c, from [69]). These features could be simulated by two continuous rotations with angles varying continuously between 0 and 5.26°; one around $[110]_\gamma$ // $[111]_\alpha$ called **A**, and the other one around $[\bar{1}11]_\gamma$ // $[\bar{1}10]_\alpha$ called **B** [1]. The **A** and **B** rotations are supposed to be the trace of the plastic accommodation of the parent phase, and are at the origin of our researches on the mechanisms of martensitic transformations [5][70]. For the fcc→bcc transformation, we have shown that the distortion matrix "contains" these two continuous rotations [1][2]: it deforms the surrounding parent environment or creates a specific back-stress field which, when the transformation continues to propagate, makes the variants deviate progressively from their initial strict OR with the parent grain. Gradients of ORs linking the Pitsch, KS and NW ORs appear inside each martensitic variant [71]. Since the concept of distortion matrices can be enlarged to all the phase transitions in the fcc-hcp-bcc system, our model predicts the existence of similar continuous features in the pole figures created by displacive transformation (fcc→hcp, hcp→bcc etc. and also mechanical twinning in fcc, hcp or bcc crystals). Theoretical and experimental works are in progress to check the validity of this prediction.

7.5. The intermediate states and the steric barriers

Since the HPs are calculated with the matrices of complete transformation, the interest of calculating the intermediate states can be questioned. Two answers can be given. First, the analytical calculations give the displacements of all the atoms *during* the transition, and not only after the transition as it is the cases in the other theories. Secondly, the matrices can be used to find an energy criterion similar to Patel and Cohen's one [72] to predict variant selection and texture inheritance effects. The interaction energy given by the tensor product of the distortion matrix by the applied stress matrix can be used. For the moment, as example, it can be noticed that a dilatation normal to the untilted plane appears during the transformation in the intermediate states, and then come back to zero in the final state (contrarily to the invariant plane strain used in PTMC). This means that there is a steric energy barrier required to "activate" the intermediate states. This situation is illustrated in Fig. 12 in the case of a 2D twinning. Although the applied stress is a simple shear, the atoms can't be sheared, and a dilatation δ should occur perpendicularly to the shear plane. The deformation is not a simple shear but is angular-distortive, which also means that due to the hard-sphere assumption the crystallographic strain-stress correlation is not linear. The calculation of the energy barrier is difficult to perform because it depends on the mechanical properties of the parent matrix and daughter variants; but the amplitude of the steric barrier δ can be calculated from the distortion matrix. In the case of fcc→fcc twinning treated in section 3, it can be checked that $\mathbf{D}_0^{\gamma\to\gamma}$ in equation (17) lets invariant the two directions $[110]_\gamma$ and $[101]_\gamma$, and thus any linear combination of them; and $\mathbf{D}_0^{*}(\eta)$ lets invariant the $(\bar{1}11)_\gamma$ plane: the crystallographic distortion associated with twinning is an invariant plane strain. However, the continuous path is not a simple shear because there is a lattice dilatation due to the

fact that the atom located in M must climb between the atoms O and K (Fig. 13b); it is given by δ = MH/($\sqrt{3}$/3), which also corresponds to the variation of the distance between the planes $\mathbf{g} = (\bar{1}11)_\gamma$, or more explicitly:

$$\frac{1}{\delta} = \frac{\|(\mathbf{D}_0^{\alpha\to\varepsilon})^*\mathbf{g}\|}{\|\mathbf{g}\|} \text{ , with } \mathbf{g} = (\bar{1}11)_\gamma \qquad (54)$$

The values of the dilatation δ have been calculated along the distortion path: they are shown in Fig. 13b. The maximum value is δ_{max}= ($\sqrt{6}$/4)/(1/$\sqrt{3}$) = 3$\sqrt{2}$/4 ≈ 1.06, which means that there is a dilatation of + 6 % perpendicularly to the twinning plane. In other words twinning can't be obtained at constant volume although the initial and final states have the same volume. There is a steric barrier between the two states due to the 6 % of volume change of the intermediate state. For fcc→bcc transformations the maximum value is δ_{max} = 1.015 (Fig. 13a); this is lower than with twinning because of the atoms O and K do not remain in contact during the climb of the atom M due to the 60°→70.5° opening angle (OPK). In real iron alloys, the hard-sphere packing rule is not strictly respected, and the theoretical expansion of +1.5 % perpendicular to the $(\bar{1}11)_\gamma$ plane in the intermediate state is actually compensated by the fact that the diameter of iron atoms is ~3% smaller in the final bcc phase than in the initial fcc parent phase. Future investigations are required to check if these calculations could respond to the question: why metastable austenite in some steels can be deformed by fcc→bcc martensitic transformation (TRIP effect), and why other steels are deformed by fcc→hcp or fcc→fcc twinning (TWIP effect), depending on their chemical composition? Up to now, the arguments in literature involve the concept of stacking fault energy (SFE), but it is probable that SFE depends on the steric barrier δ (and not only on chemistry), which itself depends on the mean diameter of the atoms in the alloy.

7.6. Does the model apply to "slow" transformations?

There are transformations that share many characteristics with martensitic transformations but that do not occur suddenly, and these "slow" transformations have been subjected to controversies between the "shearists" and the "diffusionists". Most of the debates concern the HPs and the relief formed at polished surfaces. Here, we would like to discuss another experimental result. As told in section 7.4, we believe that the orientation gradients that can be observed in the parent phase (the continuous features in the pole figures) are the plastic trace of the transformations mechanism. Since the features formed in the bcc martensitic steels are similar to those formed in slowly cooled Cu-Zn brass, duplex steels, bcc bainitic steels and iron meteorites (in which the cooling rates are few hundreds degrees by million year), we must conclude, as the "shearists", that the mechanism is intrinsically "martensitic" whatever the speed of the transformations. However, as pointed out by the "diffusionists", the transformation in these alloys is limited by the diffusion. Indeed, the chemical composition of the product laths is slightly different from the parent phase; for example, in a duplex steel, the γ laths formed inside the δ ferritic matrix are depleted in chromium and enriched in nickel [30][31]. Thus, we adopt the current consensual opinion that the transformations in these alloys are "diffusion-limited" displacive transformations. The plausible scenario of phase transformation during cooling can described as follows: (a) in the parent phase at high temperature, since the stable daughter phase is chemically different from the parent phase, and the atoms diffuse and migrate during cooling, driven by the difference of chemical potentials between the parent and daughter

phase, (b) they form a region which has the equilibrium chemical composition of the daughter phase but still has the crystallographic structure of the parent phase, and then, suddenly (c) the region is displacively transformed into the daughter phase, as schematically illustrated in Fig. 14. The transformation can't occur progressively while each atom arrives at the interface because a critical size is required for the displacive transformation to go over the energy barrier required to create the interface and the strain field, similarly as for classical nucleation [73]. Another possible cause of the limited speed of transformation is the kinetics of displacements of the dislocations generated by the lattice distortion in the matrix. These transformation dislocations induce a back-stress field localized in front of the daughter lath or plate, which makes the transformation more difficult to propagate. At high temperatures, it is possible that the dislocations glide progressively far from the lath tip and then relax the local stress field, and this allows the continuation of the phase transformation and lath growth. In steels, the kinetics of displacement of the transformation dislocations depends on the carbon content due to a Cottrell atmosphere around them. It is possible that such an effect occurs in bainitic steels. From these considerations, it is believed that the calculations presented in this paper do not apply only to pure martensitic transformations but also to diffusion-limited martensitic transformations, such as those in brass, duplex steels, iron-nickel meteorites, and to bainitic transformations in steels, and more generally to "kinematically limited" displacive transformations. The main difference with the "shearist" school approach is that a shear is not required and does not take part to the intrinsic mechanism of the lattice change.

If one accepts the idea that fcc$\rightarrow$hcp transformations and fcc$\rightarrow$fcc microtwinning are "kinematically limited" martensitic transformations, then some experimental observations in these systems can be interpreted with another point of view. For example, it is widely admitted that in some low stacking fault iron alloys the hcp plates or fcc twins are formed by a well-organized synchronized collective motion of Shockley partial dislocations created by a pole mechanism, but there is no experimental proof of the existence of dislocations spiraling around poles (section 3). There is actually a simple way to interpret the observations: instead of considering that the dislocations are the *cause* of the transformations and that the product phase is created by the passage of the dislocations, one can actually consider that the dislocations are the *consequence* of the transformation and that they are created only to accommodate the transformation. With this point of view, even in the case of microtwinning induced by shear, Shockley partial dislocations would not be generated directly by the shear stress, but would be the consequence of the creation of the fcc twin which is thermodynamically more stable than the fcc parent crystal because of its favored orientation in the stress field.

7.7. Reversibility: crystallography, morphology and dislocations

In this paper, only the fcc-hcp-bcc system is studied because it is the only system in which the hard-sphere rules can be applied with good approximation. The transformations in this system are crystallographically irreversible. We mean that, if only crystallographic arguments are considered, the reverse transformation should give back more orientations than the initial one. More explicitly, let us imagine that a single crystal γ_0 is transformed by the $\gamma\rightarrow\alpha$ transformation into N^{α} equivalent α_i variants $i \in [1, N^{\alpha}]$, the variants α_i will generate by the $\alpha\rightarrow\gamma$ inverse transformation more orientations than the initial one γ_0. This is due to the absence of a group-subgroup relationship in crystallographically reconstructive transformations [66][74]. A mathematical demonstration was given in ref. [66]: The number N^{α} of orientational variants α_i formed by

the transformation $\gamma \rightarrow \alpha$ is given by equation (50): $N^{\alpha} = |\mathbf{G}^{\gamma}| / |\mathbf{H}^{\gamma}|$ where $|\mathbf{H}^{\gamma}|$ is the order of the intersection group. The number N^{γ} of orientational variants γ_j formed by the inverse transformation $\alpha \rightarrow \gamma$ is $N^{\gamma} = |\mathbf{G}^{\alpha}| / |\mathbf{H}^{\alpha}|$. Since $\mathbf{H}^{\gamma}$ and $\mathbf{H}^{\alpha}$ are isomorph, their orders (number of elements) are equal, i.e., $|\mathbf{H}^{\alpha}| = |\mathbf{H}^{\gamma}|$. In the case of a group-subgroup relation, $\mathbf{G}^{\alpha} = \mathbf{H}^{\alpha} \leq \mathbf{G}^{\gamma}$, and then $N^{\gamma} = 1$, which means that only the orientation of the initial parent crystal can be generated by the inverse transformation. Since this condition is not satisfied in the fcc-hcp-bcc system, the transformations should not be reversible. That is why the first papers reporting an important shape memory effect in the Fe-Mn-Si steels [75] were a real surprise, as mentioned in the end-note of paper [76]. The reason is not yet fully clarified, but is probably linked to the particular configuration of transformation dislocations. In the case of fcc→hcp transformation, the accommodation is obtained by the creation of arrays of Shockley partial dislocations that all glide on parallel $\{111\}_{\gamma}$ planes (contrarily to fcc→bcc transformations which imposes the creation of at least two sets of dislocations at the origin of the orientation gradients and continuous rotations **A** and **B**, section 7.4). If the dislocations could glide far from the daughter hcp plates and be stored in the retained austenitic matrix, it is plausible that the same dislocations could move backward to induce the reverse transformation and then generate the same fcc orientation of the parent crystal. If the dislocations can't move and remain close to the plates, the fcc-hcp transformation must continue in the plastic zones containing these dislocations, which creates gradients of orientations that are inherited back during the inverse transformation. Such phenomenon of inheritance of internal gradients of orientations induced by martensitic transformation cycles was used recently by Omori *et al.* to promote abnormal grain growth and elaborate shape memory materials with millimetric grains [37].

There is another factor that can favor the reversibility in crystallographically reconstructive transformations; it is the morphological reversibility. Indeed, we have assumed in ref. [2] and in the present paper that the HP is a plane untilted by the distortion. This means that, if for the $\gamma \rightarrow \alpha$ transformation between a parent crystal γ_i and one of its variant α_j , the HP is $(h_i k_i l_i)_{\gamma}$ // $(h_j k_j l_j)_{\alpha}$, then the HP for the reverse $\alpha \rightarrow \gamma$ transformation between the crystal α_j and its variant γ_i should be the same plane $(h_j k_j l_j)_{\alpha}$ // $(h_i k_i l_i)_{\gamma}$. In other words, the reverse transformation does not require the creation of new HPs if the transformation is obtained between the same parent/daughter crystals. That morphological effect, in addition to the storage of transformation dislocations, could possibly explain the partial reversibility of the transformations observed in the fcc-hcp-bcc system.

8. Conclusions

This paper is a generalization of our previous paper [2] which was dedicated to fcc→bcc martensitic transformation. It gives for the first time the analytical expressions of the atomic displacements and lattice distortions during the fcc→fcc twinning and during fcc→hcp, bcc→fcc and bcc→hcp displacive transformations. The resulting equations are summarized in Table 5. The main ideas are:

- The distortion matrices of complete transformations can be determined directly from the orientation relationship and an appropriate lattice correspondence. They form an algebra over the

number field $\mathbb{Q}(\sqrt{6})$. The analytical calculations of the continuous distortion matrices are more tedious and rely on the hard-sphere packing assumption.

- The distortions can't imply simple shears because it would make the atoms interpenetrate themselves.
- Shuffle is required for transformations implying the bcc→hcp and fcc→hcp phase because the hcp phase contains two atoms in its Bravais lattice.
- The habit planes are determined numerically and analytically on the assumption that they are untilted by the lattice distortion. They are in the list of the eigenvectors of the distortion matrix expressed in the reciprocal space. They compare quite well with the experimental results reported in literature, taking into consideration that there is free parameter. Further work is required to establish a criterion of choice among the eigenvectors.
- The mathematical formalism is the same for the displacive phase transformations as for the mechanical twinning. There is no fundamental crystallographic difference between these two families of phenomena. All imply a lattice angular distortion without shear or intermediate phase.
- The continuous distortion matrices allow calculating the steric barriers involved by the distortions. Even the simple case of fcc→fcc mechanical twinning produced by a simple shear stress requires to cross the steric effect (+6 %) imposed by the atoms on the parallel layers of the dense planes. For the fcc→bcc martensitic transformation, the steric barrier on these planes is lower (+1.5%).
- According to the model, the dislocations should be imagined as the consequence of the lattice distortion, and not the cause. This is the classical point of view for the fcc→bcc martensitic transformation, but for the fcc→hcp transformation and fcc→fcc microtwinning it was generally believed that it is the periodic glide of Shockley partial dislocations produced by a pole mechanism that generates the hcp phase or fcc microtwins.
- The surrounding parent phase accommodates the distortion whatever its deformation modes (glide and twin pairing). In the case of fcc→bcc and bcc→fcc transformations, the plastic accommodation is retained and appears under the form of the continuous rotations **A** and **B**. The model predicts that similar features should exist in hcp martensite, and in mechanically twinned fcc, bcc or hcp metals. A large EBSD study in titanium, zirconium, cobalt, brass, TWIP steels etc. is going on in order to check this prediction.
- A distinction is done between the distortional variants with symmetries given by $\mathbb{K}$ and the orientational variants with symmetries $\mathbb{H}$ because the distortion can induce an additional symmetry breaking not contained in the sole information given by the orientation relationship. $\mathbb{K}$ is a subgroup of $\mathbb{H}$, and both $\mathbb{K}$ and $\mathbb{H}$ are subgroups of the parent point group $\mathbb{G}$. In the case of fcc→bcc transformation with KS OR, $\mathbb{K} = \mathbb{H}$, and in the case of fcc→ hcp transformation, $\mathbb{K} < \mathbb{H}$. These notions are of prime importance to calculate the macroscopic distortion matrices generated by pairs or sets of variants. They will be used in martensitic steels to show that the untilted $\{225\}_\gamma$ planes can be made fully invariant by variant pairing [3].
- The approach probably applies to the diffusion-limited displacive and bainitic transformations.

This model gives a good qualitative and unifying approach to treat displacive transformations and mechanical twinning. Of course, it is limited by its basic assumptions and can't treat the transformations in

which the atom size changes significantly between the parent and daughter phases, or in alloys constituted by atoms of different sizes. Twinning in bcc or hcp materials have not been treated here in detail because the numerous twinning systems would have made the study more tedious, but the approach is sufficiently general to treat these cases without problem. For example, it will be shown that the angular distortive matrices calculated for the $\{10\bar{1}2\}$ twinning variants in hcp crystals explain the apparent abnormality of negative Schmidt factors [64].

Note 1:

All the distortion matrices presented in the paper have been calculated from the ORs (5). One could prefer using ORs in which the negative sign is on the indices of the directions to keep the indices of the planes positive:

- KS: $[\bar{1}10]_\gamma = [\bar{1}11]_\alpha$ and $(111)_\gamma // (110)_\alpha$
- Burgers: $[\bar{1}11]_\alpha = [100]_\varepsilon$ and $(110)_\alpha // (001)_\varepsilon$
- SN : $[\bar{1}10]_\gamma = [100]_\varepsilon$ and $(111)_\gamma // (001)_\varepsilon$

The distortion matrices $\mathbf{D}_a$ corresponding to this alternative choice of OR can be deduced from the matrices **D** presented in this paper by using the coordinate transformation matrix

$$\mathbf{P} = \begin{bmatrix} 0 & -1 & 0 \\ 1 & 0 & 0 \\ 0 & 0 & 1 \end{bmatrix}, \quad \text{and, then } \mathbf{D}_a = \mathbf{P}^{-1}\,\mathbf{D}\,\mathbf{P}.$$

Note 2:

We take the opportunity of this paper to signal a typo error in the fcc$\rightarrow$bcc distortion matrix reported in Table 1 of ref. [2] for the KS OR. The matrix is correctly written in Equation (32) of ref. [2].

Acknowledgments

I would like to show my gratitude to Prof. Roland Logé who let me continue working on this theory at LMTM. PX group is also sincerely thanked for the subsidy of the LMTM laboratory. I thank Annick Baur who pointed my attention on the fact that the analytical values of the untilted planes can be obtained by calculating the eigenvectors of **D***, and for our interesting discussions on martensitic steels and mechanics.

References

[1] C. Cayron, One-step model of the face-centred-cubic to body-centred-cubic martensitic transformation, Acta Cryst. A69 (2013) 498-509.

[2] C. Cayron, Continuous atomic displacements and lattice distortion during fcc–bcc martensitic transformation, Acta Mater. 96 (2015) 189-202.

[3] A. Baur, C. Cayron, R. Logé, A revised explanation of the {225} habit planes in martensitic steels, in preparation.

[4] W.G. Burgers, On the process of transition of the cubic-body-centered modification into the hexagonal-close-packed modification of zirconium, Physica 1 (1934) 561-586.

[5] C. Cayron, F. Barcelo, Y. de Carlan, The mechanisms of the fcc-bcc martensitic transformation revealed by pole figures, Acta Mater. 58 (2010) 1395-1402.

[6] T. Liu, T.D. Zhang, Q. Liu, Y. Zheng, Y. Su, X. Zhao, J. Yin, M. Song, D. Ping, A new nanoscale metastable iron phase in carbon steels. Sci. Rep. 5 (2015) 15331; doi: 10.1038/srep15331.

[7] C. Cayron, Comment on "A new nanoscale metastable iron phase in carbon steels" (2015) arXiv:1511.00591.

[8] C. Cayron, Multiple twinning in cubic crystals: geometric/algebraic study and its application for the identification of the $\Sigma 3^n$ grain boundaries, Acta Cryst. A63 (2007) 11-29.

[9] C. Cayron, Quantification of multiple twinning in face centred cubic materials, Acta Mater. 59 (2011) 252-262.

[10] A.H. Cottrell, B.A. Bilby, A mechanism for the growth of deformation twins in crystals, Philos. Mag. 7 (1951) 573-581.

[11] J.A. Venables, Deformation twinning in face-centred cubic metals, Philos. Mag. 6 (1961) 379-396.

[12] W.Z. Han, S.D. Wu, S.X. Li, Z.F. Zhang, Origin of deformation twinning from grain boundary in copper, Appl. Phys. Let. 92 (2008) 221909.

[13] O. Bouaziz, S. Allain, C.P. Scott, P. Cugy, D. Barbier, High manganese austenitic twinning induced plasticity steels: A review of the microstructure properties relationships, Curr. Opin. Solid State Mater. Sci. 15 (2011) 141-168.

[14] B. Mahato, S.K. Shee, T. Sahu, S. Ghosh Chowdhury, P. Sahu, D.A. Porter, L.P. Karjalainen, An effective stacking fault energy viewpoint on the formation of extended defects and their contribution to strain hardening in a Fe–Mn–Si–Al twinning-induced plasticity steel, Acta Mater. 86 (2015) 69-79.

[15] T.H. Blewitt, R.R. Coltman, J.K. Redmann, Low-Temperature Deformation of Copper Single Crystals, J. Appl. Phys. 28 (1957) 651-660.

[16] M. Niewczas, Dislocations and twinning in face centred crystals, Dislocations in Solids, ed. By FRN Nabarro and JP Hirth, Elsevier BV, pp 265-364; 2007.

[17] R.W. Cahn, Plastic deformation of alpha-uranium; twinning and slip, Acta Metall. 1 (1953) 49-70.

[18] M.A. Jaswon, D.B. Dove, Twinning properties of lattice planes, Acta Cryst. 9 (1956) 621-626.

[19] M. Bevis, A.G. Crocker, Twinning shears in lattices, Proc. Roy. Soc. A304 (1968) 123-134.

[20] W. Christian, Twinning and martensitic transformation, J. Phys. C7 (1974) 65-76.

[21] F.D. Fischer, T. Schaden, F. Appel, H. Clemens, Mechanical twins, their development and growth, Europ. J. Mech. A/Solids 22 (2003) 709-726.S. Mahajan, M.L. Green, D. Brasen, A model for the FCC→HCP transformation, its applications, and experimental evidence, Metall. Trans. 8A (1977) 283-293.

[22] J. Singh, S. Ranganathan, On the Mechanism of F.C.C.→H.C.P. Transformation, Phys. State Sol. 73 (1982) 243-248.

[23] T. Waitz, H.P. Karnthaler, The f.c.c. to h.c.p. martensitic phase transformation in CoNi studied by TEM and AFM methods, Acta Mater. 45 (1997) 837-847.

[24] J.W. Brooks, M.H. Loretto, R.E. Smallman, In situ observations of the formation of martensite in stainless steel, Acta Metall. 27 (1979) 1829-1838.

[25] N. Gey, B. Petit, M. Humbert, Electron Backscattered Diffraction Study of ε/α' Martensitic Variants Induced by Plastic Deformation in 304 Stainless Steel, Metall. Mater. Trans. 36A (2005) 3291-3299.

[26] S. Kajiwara, Characteristic features of shape memory effect and related transformation behaviour of Fe-based alloys, Mater.Sci. Engng A273–275 (1999) 67–88.

[27] P. Tolédano, G. Krexner, M. Prem, H.P. Weber, V.P. Dmitriev, Theory of the martensitic transformation in cobalt Phys. Rev. B64 (2001) 144104.

[28] N. Nakada, T. Tsuchiyama, S. Takaki, S. Hashizume, Variant Selection of Reversed Austenite in Lath Martensite ISIJ Int. 47 (2007) 1527-1532.

[29] T. Fukino, S. Tsurekawa, Y. Morizono, In-Situ Scanning Electron Microscopy/Electron Backscattered Diffraction Observation of Microstructural Evolution during a $\alpha \rightarrow \gamma$ Phase Transformation in Deformed Fe-Ni Alloy, Metall. Mater. Trans. 42A (2011) 587-593.

[30] A. Redjaïmia, G. Metauer, Diffusion controlled precipitation of austenitic bi-crystals possessing twin related orientation in the ferrite of a duplex stainless steel, J. Mater. Sci. 36 (2001) 1717-1725.

[31] Y. Ohmori, K. Nakai, H. Ohtsubo, Y. Isshiki, Mechanism of Widmanstatten austenite formation in a δ/γ duplex phase stainless steel, ISIJ Int. 35 (1995) 969-975.

[32] T.A. Schroeder, C.M. Wayman, The formation of martensite and the mechanism of the shape memory effect in single crystals of Cu-Zn alloys, Acta Metall. 25 (1977) 1375-1391.

[33] T. Saburi, C.M. Wayman, Crystallographic similarities in shape memory martensite, Acta Metall. 27 (1979) 979-995.

[34] B.C. Muddle, J.F. Nie, G.R. Hugo, Application of the Theory of Martensite Crystallography to Displacive Phase Transformations in Substitutional Nonferrous Alloys, Metall. Mater. Trans. 25A (1994) 1841-1856.

[35] G.R. Srinivasan, M.T. Hepworth, The crystallography of the bainite transformation in beta brass, Acta Metall. 19 (1971) 1121-1131.

[36] N. Stanford, P.S. Bate, Crystallographic variant selection in α–β brass, Acta Mater. 53 (2005) 859-867.

[37] T. Omori, T. Kusama, S. Kawata, I. Ohnuma, Y. Sutou, Y. Araki, K. Ishida, R. Kainuma, Abnormal Grain Growth Induced by Cyclic Heat Treatment, Science 341 (2013) 1500-1502.

[38] D. Banerjee, J.C. Williams, Perspectives on titanium science and technology, Acta Mater. 61 (2013) 844-879.

[39] N. Gey, M. Humbert, E. Gautier, J.L. Béchade, Study of the $\beta \rightarrow \alpha$ variant selection for a zircaloy-4 rod heated to the β transus in presence or not of an axial tensile stress, J. Nucl. Mater. 328 (2004) 137-145.

[40] E.C. Bain, The nature of martensite, Trans. Amer. Inst. Min. Metall. Eng. 70 (1924) 25-35.

[41] J.S. Bowles, J.K. MacKenzie. The Crystallography of Martensite Transformation IV. Body Centred Cubic to Orthorhombic transformations, Acta Metall. 5 (1957) 137-149.

[42] P. Gaunt, J.W. Christian, The crystallography of the $\beta \rightarrow \alpha$ transformation in zirconium and in the two titanium-molybdenum alloys, Acta Metall. 7 (1959) 534-543.

[43] S. Banerjee, G.K. Dey, D. Srivastava, S. Ranganathan, Plate-Shaped Transformation Products in Zirconium-Base

Alloys, Metall. Mater. Trans 28A (1997) 2201-2216.

[44] M.X. Zhang, P.M. Kelly, Edge-to-edge matching and its applications Part I. Application to the simple HCP/BCC system, Acta Mater. 53 (2005) 1073-1084.

[45] G. Kurdjumov, G. Sachs, Über den Mechanismus der Stahlhärtung, Z. Phys. 64 (1930) 325-343.

[46] J. Young, The crystal structure of meteoric iron as determined by X-ray analysis, Proc. R. Soc. London 112A (1926) 630-641.

[47] Z. Nishiyama, Martensitic Transformation, Ed. by M.E. Fine, M. Meshii, C.M. Waymann, Materials Science Series, Academic Press, New York, 1978.

[48] D. Qiu, M.X. Zhang, P.M. Kelly, T. Furuhara, Non-classical $\{334\}_{\beta}$ type of twinned α' martensite in a Ti–5.26 wt.% Cr alloy, Acta Mater. 67 (2014) 373-382.

[49] K. Otsuka, X. Ren, Physical metallurgy of Ti–Ni-based shape memory alloys, Progress Mater. Sci. 50 (2005) 511-678.

[50] P. Tolédano, V. Dmitriev, Reconstructive Phase Transitions, World Scientific Publishing Co, 1996.

[51] M.X. Zhang, P.M. Kelly, Crystallographic features of phase transformations in solids, Progress Mater. Sci. 54 (2009) 1101-1170.

[52] J.W. Christian, The theory of transformations in metals and alloys, part II, Oxford: Elsevier Science Ltd; pp 961-1113; 2002.

[53] H.K.D.H. Bhadeshia, Worked examples in the geometry of crystals, 2d ed, Brookfield, The Institute of Metals, 1987.

[54] J.S. Bowles, J.K. MacKenzie, The Crystallography of Martensite Transformations I, Acta Metall. 2 (1954) 129-137.

[55] Z. Nishiyama, Martensitic Transformation, Ed. by M.E. Fine, M. Meshii, C.M. Waymann, Materials Science Series, Academic Press, New York, 1978.

[56] K. Bhattacharya, Microstructure of martensite, why it forms and how it gives rise to the shape-memory effect, Oxford University Press, Oxford, 2003.

[57] H.I. Aaronson, G. Spanos, R.A. Masamura, R.G. Vardiman, D.W. Moon, E.S.K. Menon, M.G. Hall, Sympathetic nucleation: an overview, Mater. Sci. Engng B32 (1995) 107-123.

[58] T. Furuhara, T. Ogawa, T. Maki, Surface relief effect and atomic site correspondence in the grain boundary α precipitation in a β Ti-Cr alloy, Scripta Mater. 34 (1996) 381-386.

[59] S.P. Ringer, K. Hono, Microstructural evolution and age hardening in aluminium alloys: atom probe field-ion microscopy and transmission electron microscopy studies, Mater. Charact. 44 (2000) 101-131.

[60] C. Cayron, P.A. Buffat, Transmission electron microscopy study of the β' phase (Al–Mg–Si alloys) and QC phase (Al–Cu–Mg–Si alloys): ordering mechanism and crystallographic structure, Acta Mater. 48 (2000) 2639-2653.

[61] G. Friedel, Etude sur les groupements cristallins: Extrait du Bulletin de la Société de l'Industrie Minérale, Quatrième Série, Tomes III et IV. Saint Etienne, Imprimerie Théolier J. et Cie, 1904.

[62] T. Hahn, H. Klapper, Twinning of Crystals, in: A. Authier (Ed.), International Tables for Crystallography, vol. D. Boston, Kluwer Academic Publishers, 2003, pp 393-448.

[63] K. D. Molodov, T. Al-Samman, D.A. Molodov, G. Gottstein, On the role of anomalous twinning in the plasticity of magnesium, Acta Mater. 103 (2016) 711-723.

[64] C. Cayron, The apparent anomaly of {10-12} twinning in HCP metals explained by the angular distortive matrices, in preparation.

[65] J.W. Cahn, G. Kalonji, Solid-Solid Phase Transformations, Ed. by H. I. Aaronson, D. E. Laughlin, R. F. Skerka & C. M. Marvin Wayman, Washington: The Metallurgical Society of AIME; 1981. pp. 3–14.

[66] C. Cayron, Groupoid of orientational variants, Acta Cryst. A62 (2006) 21-40.

[67] N. Bergeon, G. Guenin, C. Esnouf, Microstructural analysis of the stress-induced of martensite in a Fe–Mn–Si–Cr–Ni shape memory alloy: Part I—calculated description of the microstructure, Mater. Sci. Engng A242 (1998) 77-86.

[68] M.U. Farooq, U. Klement, G. Nolze, The role of α to ε-Co phase transformation on strain hardening of a Co–Cr–Mo laser clad, Mater. Sci. Engng A445-446 (2007) 40-47.

[69] W. Zielinski, W. Swiatnicki, Measurements of duplex steel, in Calendar 2002, HKL Technology. Reported in G. Nolze, V. Geist, A new method for the investigation of orientation relationships in meteoritic plessite, Cryst. Res. Technol. 39 (2004) 343-352.

[70] C. Cayron, F. Barcelo, Y. de Carlan, Reply to "comments on 'The mechanisms of the fcc-bcc martensitic transformation revealed by pole figures' ", Scripta Mater. 64 (2011) 103-106.

[71] C. Cayron, EBSD imaging of orientation relationships and variant groupings in different martensitic alloys and Widmanstätten iron meteorites, Mater. Charact. 94 (2014) 93-110.

[72] J.R. Patel, M. Cohen, Criterion for the action of applied stress in the martensitic transformation Acta Metall 1 (1953) 531-538.

[73] L. Delaey, Materials Science and Technology : A Comprehensive Treatment. Phase Transformations in Materials, Diffusionless Transformations, R.W. Cahn, P. Hassen and EJ Kramer (Eds.), vol. 5, VCH, 1996.

[74] K. Bhattacharya, S. Conti, G. Zanzotto, J. Zimmer, Crystal symmetry and the reversibility of martensitic transformations, Nature 428 (2004) 55-59.

[75] Y. Tanaka, Y. Himuro, R. Kainuma, Y. Sutou, T. Omori, K. Ishida, Ferrous Polycrystalline Shape-Memory Alloy Showing Huge Superelasticity, Science 327 (2010) 1488-1490.

[76] K. Otsuka, A. Saxena, J. Deng, X. Ren, Mechanism of the shape memory effect in martensitic alloys: an assessment, Phil. Mag. 91 (2011) 4514-4535.

TABLES

$\mathbf{T}_0^{\gamma\to\alpha} = \begin{pmatrix} \frac{1}{3\sqrt{6}} & \frac{1}{18}(12+\sqrt{6}) & \frac{1}{9}(3-\sqrt{6}) \\ \frac{2}{3}-\frac{1}{3\sqrt{6}} & -\frac{1}{3\sqrt{6}} & \frac{1}{9}(3+\sqrt{6}) \\ \frac{1}{9}(3+\sqrt{6}) & \frac{1}{9}(-3+\sqrt{6}) & -\frac{2\sqrt{\frac{2}{3}}}{3} \end{pmatrix}$	$\mathbf{T}_0^{\alpha\to\gamma} = \begin{pmatrix} \frac{1}{2\sqrt{6}} & 1-\frac{1}{2\sqrt{6}} & \frac{1}{2}+\frac{1}{\sqrt{6}} \\ 1+\frac{1}{2\sqrt{6}} & -\frac{1}{2\sqrt{6}} & -\frac{1}{2}+\frac{1}{\sqrt{6}} \\ \frac{1}{2}-\frac{1}{\sqrt{6}} & \frac{1}{2}+\frac{1}{\sqrt{6}} & -\sqrt{\frac{2}{3}} \end{pmatrix}$
$\mathbf{T}_0^{\gamma\to\varepsilon} = \begin{pmatrix} \frac{1}{2} & 0 & \frac{2}{3} \\ \frac{1}{2} & -\frac{1}{2} & -\frac{2}{3} \\ 0 & \frac{1}{2} & -\frac{2}{3} \end{pmatrix}$	$\mathbf{T}_0^{\varepsilon\to\gamma} = \begin{pmatrix} \frac{4}{3} & \frac{2}{3} & \frac{2}{3} \\ \frac{2}{3} & -\frac{2}{3} & \frac{4}{3} \\ \frac{1}{2} & -\frac{1}{2} & -\frac{1}{2} \end{pmatrix}$
$\mathbf{T}_0^{\alpha\to\varepsilon} = \begin{pmatrix} \frac{1}{2} & \frac{1}{8}(-2+\sqrt{6}) & -1 \\ \frac{1}{2} & \frac{1}{8}(-2+\sqrt{6}) & 1 \\ \frac{1}{2} & \frac{1}{4}(-1-\sqrt{6}) & 0 \end{pmatrix}$	$\mathbf{T}_0^{\varepsilon\to\alpha} = \begin{pmatrix} \frac{1}{9}(6+\sqrt{6}) & \frac{1}{9}(6+\sqrt{6}) & -\frac{2}{9}(-3+\sqrt{6}) \\ \frac{2}{3}\sqrt{\frac{2}{3}} & \frac{2}{3}\sqrt{\frac{2}{3}} & -\frac{4}{3}\sqrt{\frac{2}{3}} \\ -\frac{1}{2} & \frac{1}{2} & 0 \end{pmatrix}$

Table 1 Coordinate transformation matrices between the fcc (γ), bcc (α) and hcp (ε) phases for KS, Burgers and NS ORs.

Images of directions	
3 $<100>_\alpha$	1 $<100>_\gamma$ 2 $<110>_\gamma$
6 $<110>_\alpha$	4 $<211>_\gamma$ 2 $<100>_\gamma$
4 $<111>_\alpha$	4 $<110>_\gamma$
12 $<112>_\alpha$	8 $<123>_\gamma$ 4 $<210>_\gamma$
Images of planes	
3 $\{100\}_\alpha$	1 $\{100\}_\gamma$ 2 $\{110\}_\gamma$
6 $\{110\}_\alpha$	4 $\{111\}_\gamma$ 2 $\{100\}_\gamma$
4 $\{111\}_\alpha$	4 $\{210\}_\gamma$
12 $\{112\}_\alpha$	8 $\{113\}_\gamma$ 4 $\{110\}_\gamma$

Table 2 Images of low-index directions and planes by the bcc→fcc transformation with KS OR.

Images of directions	
3 $\langle 100 \rangle_{\alpha}$	$2\langle 211 \rangle_{\varepsilon}$ 1 $\langle 100 \rangle_{\varepsilon}$
6 $\langle 110 \rangle_{\alpha}$	2 $\langle 2\text{-}11 \rangle_{\varepsilon}$ 2 $\langle 230 \rangle_{\varepsilon}$ 1 $\langle 210 \rangle_{\varepsilon}$ 1 $\langle 001 \rangle_{\varepsilon}$
4 $\langle 111 \rangle_{\alpha}$	2 $\langle 100 \rangle_{\varepsilon}$ 2 $\langle 101 \rangle_{\varepsilon}$
Images of planes	
3 $\{100\}_{\alpha}$	2 $\{102\}_{\varepsilon}$ 1 $\{120\}_{\varepsilon}$
6 $\{110\}_{\alpha}$	2 $\{101\}_{\varepsilon}$ 2 $\{210\}_{\varepsilon}$ 1$\{100\}_{\varepsilon}$ 1$\{001\}_{\varepsilon}$
4 $\{111\}_{\alpha}$	2 $\{1\text{-}24\}_{\varepsilon}$ 1 $\{3\text{-}20\}_{\varepsilon}$ 1 $\{120\}_{\varepsilon}$

Table 3 Images of low-index directions and planes by the bcc→hcp transformation with Burgers OR.

Transformation	$\gamma \rightarrow \alpha$	$\alpha \rightarrow \gamma$
Point group of the parent phase	$\mathfrak{G}^{\gamma}$	$\mathfrak{G}^{\alpha}$
Orientational variants		
Coordinate-transformation matrix (Orientation Relationship)	$\mathbf{T}_0^{\gamma\rightarrow\alpha}$	$\mathbf{T}_0^{\alpha\rightarrow\gamma} = (\mathbf{T}_0^{\gamma\rightarrow\alpha})^{-1}$
Intersection group	$\mathfrak{H}^{\gamma} = \mathfrak{G}^{\gamma} \cap \mathbf{T}_0^{\gamma\rightarrow\alpha}\,\mathfrak{G}^{\alpha}\,(\mathbf{T}_0^{\gamma\rightarrow\alpha})^{-1}$	$\mathfrak{H}^{\alpha} = \mathfrak{G}^{\alpha} \cap \mathbf{T}_0^{\alpha\rightarrow\gamma}\,\mathfrak{G}^{\gamma}\,(\mathbf{T}_0^{\alpha\rightarrow\gamma})^{-1} \equiv \mathfrak{H}^{\gamma}$
Orientational variants	$\alpha_i\,\mathbf{T}_0^{\gamma\rightarrow\alpha}, \quad \alpha_i \in \mathfrak{G}^{\gamma}/\mathfrak{H}^{\gamma}$	$\gamma_i\,\mathbf{T}_0^{\alpha\rightarrow\gamma}, \quad \gamma_i \in \mathfrak{G}^{\alpha}/\mathfrak{H}^{\alpha}$
Number of orientational variants	$N^{\alpha} = \lvert\mathfrak{G}^{\gamma}\rvert / \lvert\mathfrak{H}^{\gamma}\rvert$	$N^{\gamma} = \lvert\mathfrak{G}^{\alpha}\rvert / \lvert\mathfrak{H}^{\alpha}\rvert$
Link between the numbers of orientational variants for direct/inverse transformations	$N^{\alpha}\,\lvert\mathfrak{G}^{\alpha}\rvert = N^{\gamma}\,\lvert\mathfrak{G}^{\gamma}\rvert$	
Distortional variants		
Distorsion matrix	$\mathbf{D}_0^{\gamma\rightarrow\alpha}$	$\mathbf{D}_0^{\alpha\rightarrow\gamma} = \mathbf{T}_0^{\alpha\rightarrow\gamma}(\mathbf{D}_0^{\gamma\rightarrow\alpha})^{-1}\,\mathbf{T}_0^{\gamma\rightarrow\alpha}$
Intersection group	$\mathfrak{K}^{\gamma} = \mathfrak{G}^{\gamma} \cap \mathbf{D}_0^{\gamma\rightarrow\alpha}\,\mathfrak{G}^{\gamma}\,(\mathbf{D}_0^{\gamma\rightarrow\alpha})^{-1}$	$\mathfrak{K}^{\alpha} = \mathfrak{G}^{\alpha} \cap \mathbf{D}_0^{\alpha\rightarrow\gamma}\mathfrak{G}^{\alpha}\,(\mathbf{D}_0^{\alpha\rightarrow\gamma})^{-1}$
Distortional variants	$d_i^{\alpha}\,\mathbf{D}_0^{\gamma\rightarrow\alpha}, \quad d_i^{\alpha} \in \mathfrak{G}^{\gamma}/\mathfrak{K}^{\gamma}$	$d_i^{\gamma}\,\mathbf{D}_0^{\alpha\rightarrow\gamma}, \quad d_i^{\gamma} \in \mathfrak{G}^{\alpha}/\mathfrak{K}^{\alpha}$
Number of distortional variants	$M^{\alpha} = \lvert\mathfrak{G}^{\gamma}\rvert / \lvert\mathfrak{K}^{\gamma}\rvert$	$M^{\gamma} = \lvert\mathfrak{G}^{\alpha}\rvert / \lvert\mathfrak{K}^{\alpha}\rvert$
Link between the habit planes for direct/inverse transformations	$(h_i k_i l_i)_{\gamma} \,//\, (h_j k_j l_j)_{\alpha}$	

Table 4 Crystallographic definition properties of orientation and distortion shape variants for direct and inverse transformations. Different distortion matrices lead to different distorted shapes but can lead to the same orientation of the daughter crystals, as it is the case for fcc→hcp transformation (section 7.1), that is why, for such transformations, the orientational and distortional variants should be distinguished. Generally, $\mathfrak{K}^{\gamma}$ is a subgroup of the intersection group $\mathfrak{H}^{\gamma}$, $\mathfrak{K}^{\gamma} \leq \mathfrak{H}^{\gamma}$. For fcc→hcp transformations $\mathfrak{K}^{\gamma} < \mathfrak{H}^{\gamma}$. For fcc-bcc transformations $\mathfrak{K}^{\gamma} = \mathfrak{H}^{\gamma}$.

Transition	**OR**	**Complete distortion matrix**	**Continuous distortion matrix**	**Shuffle**	**Predicted HPs (rationalized)**	**Observed HPs (reported in literature)**	**Difference**
fcc→ bcc	KS	Equ. (31) of ref. [2]	Equ. (32) of ref. [2]	No	$(\bar{1}11)_\gamma$ $(\bar{2}25)_\gamma$	$(\bar{1}11)_\gamma$ $(\bar{2}25)_\gamma$	0° 0.5°
fcc → fcc	Twin	Equ. (11)	Equ. (17)	No	$(\bar{1}11)_\gamma$	$(\bar{1}11)_\gamma$	0°
fcc→ hcp	NS	Equ. (22)	Equ. (25)	Equ. (27) + (28)	$(\bar{1}11)_\gamma$	$(\bar{1}11)_\gamma$	0°
bcc → fcc	KS	Equ. (31)	Equ. (37)	No	$(\bar{1}10)_\alpha$ $(\bar{5}32)_\alpha$	$(\overline{12},11,2)_\alpha$ $(\bar{3}21)_\alpha$	7.4° 4.3°
bcc→ hcp	Burgers	Equ. (40)	Equ. (45)	Equ. (47) + (48)	$(\bar{1}10)_\alpha$ $(\bar{1}\bar{1}2)_\alpha$ $(\bar{5}\bar{5}4)_\alpha$	- - $(\bar{4}\bar{4}3)_\alpha$ $(\bar{4}\bar{4}5)_\alpha$	- - 1.5° 12°

Table 5 Summary of the equations obtained in the paper. The details of the KS, NS and Burgers ORs are given in the equations (5). It is recalled that γ = FCC, α = BCC and ε = HCP. Only the rationalized values of the predicted habit planes are noted in the table in order to simplify the table. The exact irrational values of the HPs are $(\bar{1}1\sqrt{6})_\gamma \approx (\bar{2}25)_\gamma$ for the fcc→bcc transition, $(-7-2\sqrt{6},2+2\sqrt{6},5)_\alpha \approx (\bar{5}32)_\alpha$ for the bcc→fcc transition, and $(-\sqrt{6},-\sqrt{6},2)_\alpha \approx (\bar{5}\bar{5}4)_\alpha$ for the bcc→hcp transition.

FIGURE CAPTIONS

Fig. 1. *Phase transformations in the fcc-hcp-bcc system. (a) As represented by Burgers in 1934 [4]. (b) Planar representation of the fcc, bcc and hcp lattices with the orientation relationship conventions used in the paper. The positions l = 1 and l = 2 represent the level of the atom in the stacking of the dense planes* $(\bar{1}11)_\gamma // (\bar{1}10)_\alpha // (001)_\varepsilon$.

Fig. 2. *Fcc→ fcc twinning on the* $(\dot{1}11)_\gamma$ *plane. The plane* $(\dot{1}11)_\gamma$ *is marked by the POK triangle, before twinning, with* $\mathbf{P0} = ½\,[110]_\gamma$, $\mathbf{PK} = ½\,[101]_\gamma$, $\mathbf{PM} = [100]_\gamma$, $\mathbf{OK} = ½\,[0\dot{1}1]_\gamma$, $\mathbf{PJ} = ¼\,[211]_\gamma$ *and* $\mathbf{JM} = ¼\,[2\dot{1}\dot{1}]_\gamma$. *The point J is in the middle of OK and the point H is the projection of M on the PJ line. The triangle POK is unchanged by twinning (β = 60°), contrarily to fcc→bcc transformation. The atom in M, initially such that* $\mathbf{PM} = [100]_\gamma$, *moves and passes over the atoms in O and K, and goes to its final twinning position, located such that the tetrahedron POKM is regular. During this displacement, the angle η = 2γ varies from η = arcos(1/3)=70.5° to η = - arcos(1/3) = 180° - 70.5° = 109.5°. (a) 3D view of the fcc cube, (b) part of this cube indicating the intermediate basis used in the calculations (**x** = **PO**, **y** = **PK**, **z** = **PM**). (c) 2D section of (b) on the PJM plane.*

Fig. 3. *Views on the* $(0\dot{1}1)_\gamma$ *and* $(1\dot{1}\dot{1})_\gamma$ *plane of the transformation of a fcc crystal into (a) bcc , (b) mechanically twinned fcc, or (c) hcp crystal, with KS, twin or SN OR, respectively. The purple arrows correspond to the atomic displacements that follow the lattice distortion, and the green arrow in (c) represents the shuffle of the atom M. In (c), M moves in the position previously occupied by N, while N moves to the position above the atom P at level l=2. Another possibility of shuffle is that M stays locally at the same place in its unit cell.*

Fig. 4. *3D representations of (a) fcc→ bcc martensitic transformation, (b) fcc→ fcc mechanical twinning, and (c) fcc→ hcp martensitic transformation, with, in blue, the initial parent fcc cube with its* $\{100\}_\gamma$ *facets, in red, the resulting transformed daughter crystals, and in yellow, the intermediate states stopped at medium path (half of the maximum distortion angle). The black arrow represents the invariant neutral line* $[110]_\gamma$, *and the white arrow the* $[101]_\gamma$ *direction (also invariant for the fcc→ hcp and fcc→ fcc transformations).*

Fig. 5. *Lattice used for the bcc→ fcc and bcc→ hcp transformations. (a) The triangle POK corresponds to the same triangle as used for the fcc→ bcc transformation. The directions PO and PK are the close-packed directions* $\mathbf{PO} = ½\,[111]_\alpha$ *and* $\mathbf{PK} = ½\,[11\dot{1}]_\alpha$. *(b) The angle β between these two directions changes from β = 70.5° (bcc) to β = 60° (fcc). In the final state (fcc), the atoms O and K are in contact. The atom M is*

such that $\boldsymbol{PM} = [010]_\alpha$. *The projection of M on the plane POK =* $(\bar{1}10)_\alpha$ *is J such that in the bcc structure* $\boldsymbol{JM} = ½\,[\bar{1}10]_\alpha$. *(c) During the bcc → fcc transformation, the atom of the bcc phase initially in position* M^α *shuffles to the position* M^γ *of the fcc phase. The shortening of the distance OK is not visible in (c) because it is perpendicular to PJ. Two equivalent shuffles in opposite directions are possible.*

Fig. 6. *Views on the* $(00\bar{1})_\alpha$ *and* $(\bar{1}10)_\alpha$ *planes of the transformation of a bcc crystal into (a) fcc or (b) hcp crystal, with KS or SN OR, respectively. The purple arrows correspond to the atomic displacements that follow the lattice distortion, and the green arrow in (b) is a shuffle. Only one of the two possible shuffles is represented in (b). The atom in M could also have moved in the opposite direction, as shown in Fig. 5c.*

Fig. 7. *Determination of the untilted planes of the bcc→ fcc transformations. (a) Graphical representations of* $\| \boldsymbol{\Delta g}_\perp \|$ *given in %. (a) 2D representation according to the spherical coordinates* θ *and* φ, *with* $\theta \in [0,\pi]$ *and* $\theta \in [0,2\pi]$. *(b) Enlargement of the region around the two local minima* $(\bar{1}10)_\alpha$ *and* $(-7-2\sqrt{6},\ 2+2\sqrt{6},\ 5)_\alpha \approx (\bar{5}32)_\alpha$.

Fig. 8. *Determination of the untilted planes of the bcc→hcp transformation. (a) Graphical representation of* $\| \boldsymbol{\Delta g}_\perp \|$ *given in %. (a) 2D representation according to the spherical coordinates* θ *and* φ, *with* $\theta \in [0,\pi]$ *and* $\theta \in [0,2\pi]$. *The local minima* $(\bar{1}10)_\alpha$, $(\bar{1}\bar{1}2)_\alpha$ *and* $(-\sqrt{6},\ -\sqrt{6},\ 2)_\alpha \approx (\bar{5}\bar{5}4)_\alpha$

Fig. 9. *3D representations of (a) bcc→ fcc and (b) bcc→ hcp transformations, with, in blue, the initial parent bcc crystal cube with its* $\{100\}_\alpha$ *facets, in red, the resulting transformed daughter crystals, and in yellow, the intermediate states stopped at medium path (half of the distortion angle). The black arrow represents the invariant neutral line* $[111]_\alpha$, *and the white arrow the* $[11\bar{1}]_\alpha$ *direction (rotated by both transformations).*

Fig. 10. *Difference of fcc→ hcp transformation mechanism between (a,c) precipitation and (b,d) martensitic transformation. The schematic representations are oriented edge-on along* $[\bar{1}11]_\gamma$ *in (a,b), and on the side along* $[110]_\gamma$ *in (b,d). The point group of the shape of the precipitates is* $\boldsymbol{H}$. *The point group of the shape of the martensitic variants is* $\boldsymbol{K}$; *it is a subgroup of* $\boldsymbol{H}$.

Fig. 11. *Similarities of the continuous features observed in the EBSD pole figures of (a) the* $<110>_{bcc}$ *directions formed by the martensitic laths in a parent fcc grain of a martensitic steel (EM10, thermally treated), (b) the* $<110>_{fcc}$ *directions formed by the laths of a Widmanstätten colony in a parent bcc grain of a brass alloy (from [36]), and (c) the* $<110>_{fcc}$ *directions formed by the martensitic austenite laths in a parent* δ *bcc grain, in a duplex steel (from[69]). The three-fold "flower" and four-fold "cross" are identified by the large and medium size circles.*

Fig. 12. *Schematic 2D representation of the intermediate states and steric barriers. (a) The ($\mathbf{a}_1$,$\mathbf{b}_1$) basic vectors of the lattice 1 are transformed by twinning into the ($\mathbf{a}_2$,$\mathbf{b}_2$) basic vector of the lattice 2 by the application of a shear stress* $\mathbf{s}$*. (b) Due to the hard-sphere packing the resulting deformation is not a simple shear strain but an angular distortion, and a slight dilatation component* δ *naturally appears during the transformation; it is maximum in the intermediate state in red.*

Fig. 13. *Comparison between (a) martensitic transformation and (b) twinning, with a 3D representation of the hard-sphere atoms. The letters P, O, K, M are at the centres of the atoms, as in ref. [2]. The curves at the right side represent the variation of the spacing of the* $(\bar{1}11)_\gamma$ *plane during the transformation, i.e. when the angular order parameter changes from* $\beta = 60°$ *to 70.5° for martensite, and from* $\eta = 70.5°$ *to 109.5° for twinning.*

Fig. 14. *Schematic representation of a diffusion-limited displacive transformation. First, the chemical composition of the daughter phase is obtained by a slow process of atomic diffusion, but the crystallographic structure is still the parent phase one, and then, when the critical size is reached, the transformation suddenly (and displacively) occurs. The distortion introduces dislocations in the surrounding parent matrix. The kinetics of the displacements of these dislocations created at the tip of the plate can also influence the kinetics of transformation.*

FIGURES

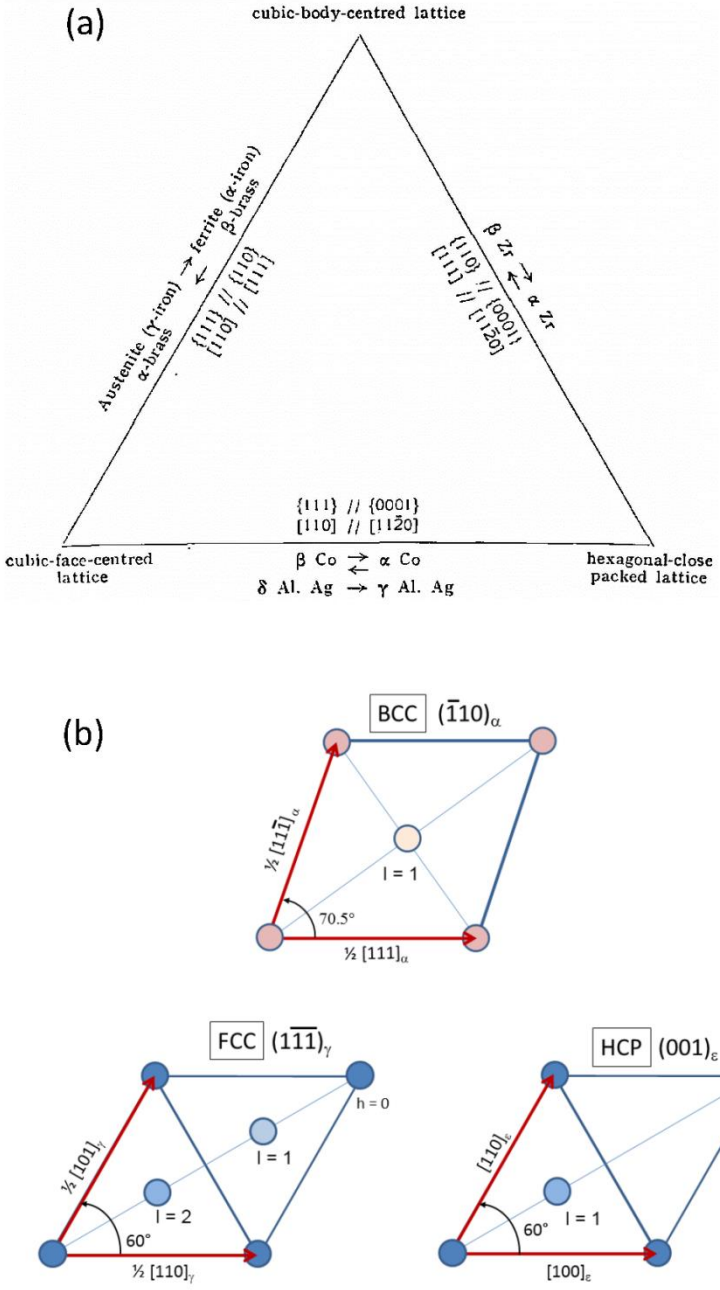

Fig. 1. *Phase transformations in the fcc-hcp-bcc system. (a) As represented by Burgers in 1934 [4]. (b) Planar representation of the fcc, bcc and hcp lattices with the orientation relationship conventions used in the paper. The positions l = 1 and l = 2 represent the level of the atom in the stacking of the dense planes* $(\bar{1}11)_\gamma // (\bar{1}10)_\alpha // (001)_\varepsilon$.

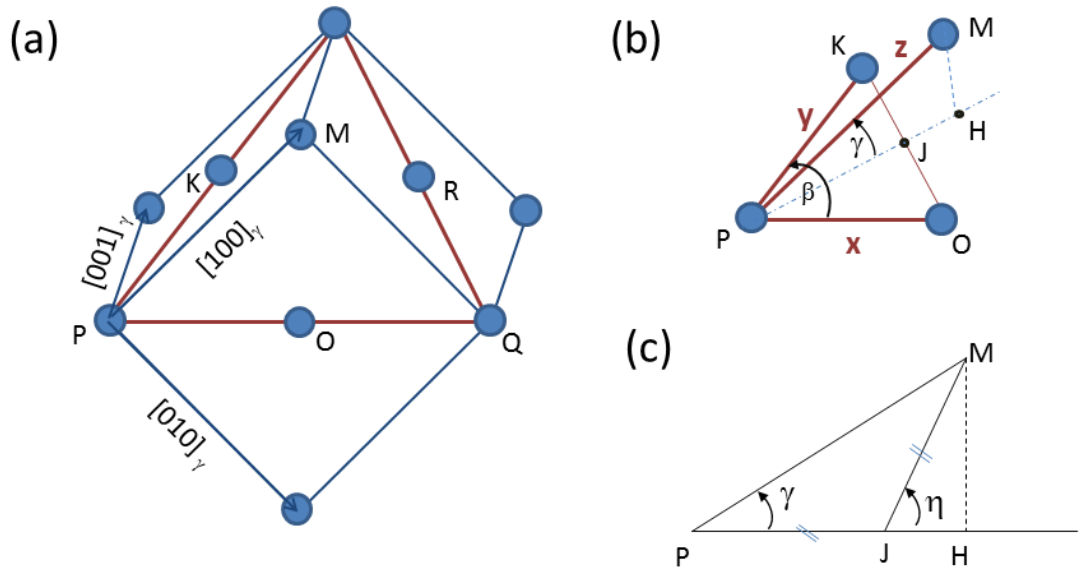

Fig. 2. *Fcc→fcc twinning on the* $(\bar{1}11)_\gamma$ *plane. The plane* $(\bar{1}11)_\gamma$ *is marked by the POK triangle, before twinning, with* ***P0*** *= ½* $[110]_\gamma$ *,* ***PK*** *= ½* $[101]_\gamma$ *,* ***PM*** *=* $[100]_\gamma$*,* ***OK*** *= ½* $[0\bar{1}1]_\gamma$ *,* ***PJ*** *= ¼* $[211]_\gamma$ *and* ***JM*** *= ¼* $[2\bar{1}\bar{1}]_\gamma$*. The point J is in the middle of OK and the point H is the projection of M on the PJ line. The triangle POK is unchanged by twinning (β = 60°), contrarily to fcc→bcc transformation. The atom in M, initially such that* ***PM*** *=* $[100]_\gamma$ *, moves and passes over the atoms in O and K, and goes to its final twinning position, located such that the tetrahedron POKM is regular. During this displacement, the angle η = 2γ varies from η = arcos(1/3)=70.5° to η = - arcos(1/3) = 180° - 70.5° = 109.5°. (a) 3D view of the fcc cube, (b) part of this cube indicating the intermediate basis used in the calculations (****x*** *=* ***PO****,* ***y*** *=* ***PK****,* ***z*** *=* ***PM****). (c) 2D section of (b) on the PJM plane.*

(a)

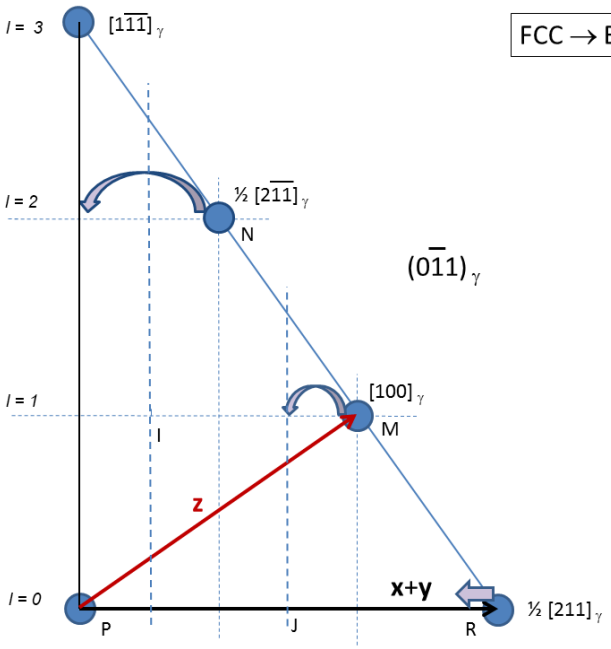
FCC → BCC (KS)
l = 3
[1$\bar{1}\bar{1}$]γ
l = 2
½ [2$\bar{1}\bar{1}$]γ
N
(0$\bar{1}$1)γ
l = 1
[100]γ
M
I
z
l = 0
x+y
½ [211]γ
P
J
R

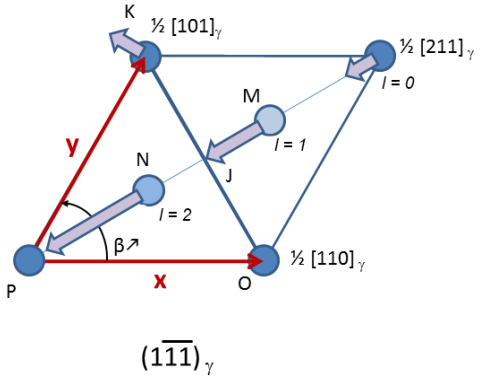
K
½ [101]γ
½ [211]γ
l = 0
M
l = 1
y
N
J
l = 2
β
½ [110]γ
P
x
O
(1$\bar{1}\bar{1}$)γ

(b)

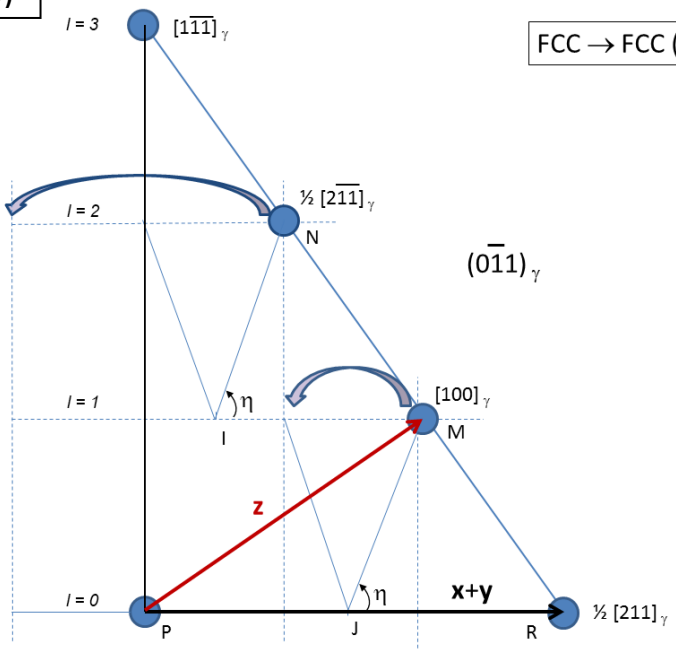
FCC → FCC (twinning)
l = 3
[1$\bar{1}\bar{1}$]γ
l = 2
½ [2$\bar{1}\bar{1}$]γ
N
(0$\bar{1}$1)γ
l = 1
η
[100]γ
M
I
z
l = 0
η
x+y
½ [211]γ
P
J
R

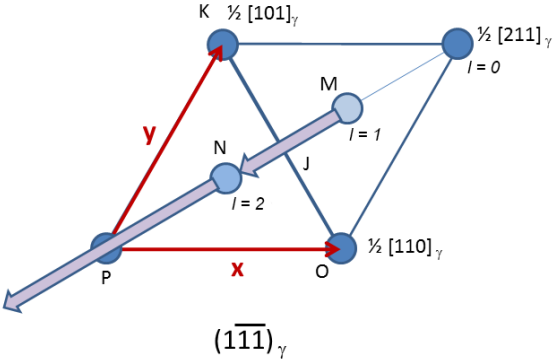
K
½ [101]γ
½ [211]γ
l = 0
M
l = 1
y
N
J
l = 2
½ [110]γ
P
x
O
(1$\bar{1}\bar{1}$)γ

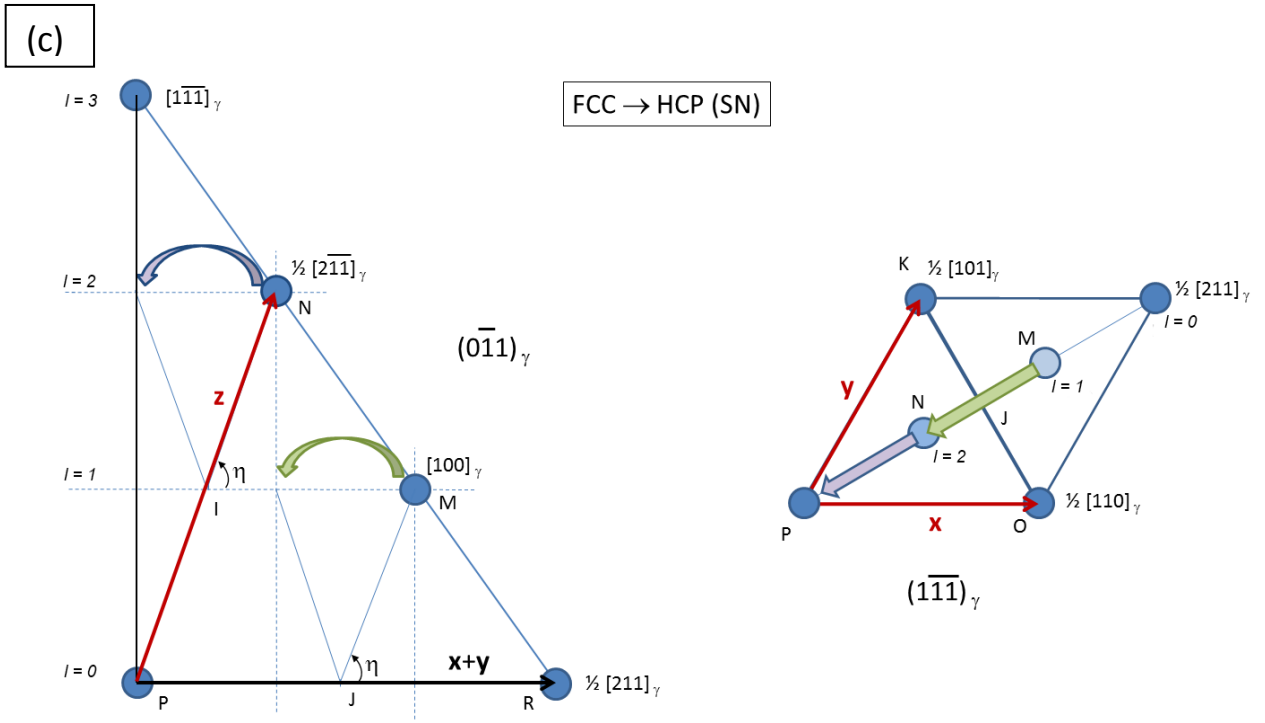

Fig. 3. *Views on the $(0\bar{1}1)_\gamma$ and $(1\bar{1}\bar{1})_\gamma$ plane of the transformation of a fcc crystal into (a) bcc , (b) mechanically twinned fcc, or (c) hcp crystal, with KS, twin or SN OR, respectively. The purple arrows correspond to the atomic displacements that follow the lattice distortion, and the green arrow in (c) represents the shuffle of the atom M. In (c), M moves in the position previously occupied by N, while N moves to the position above the atom P at level l=2. Another possibility of shuffle is that M stays locally at the same place in its unit cell.*

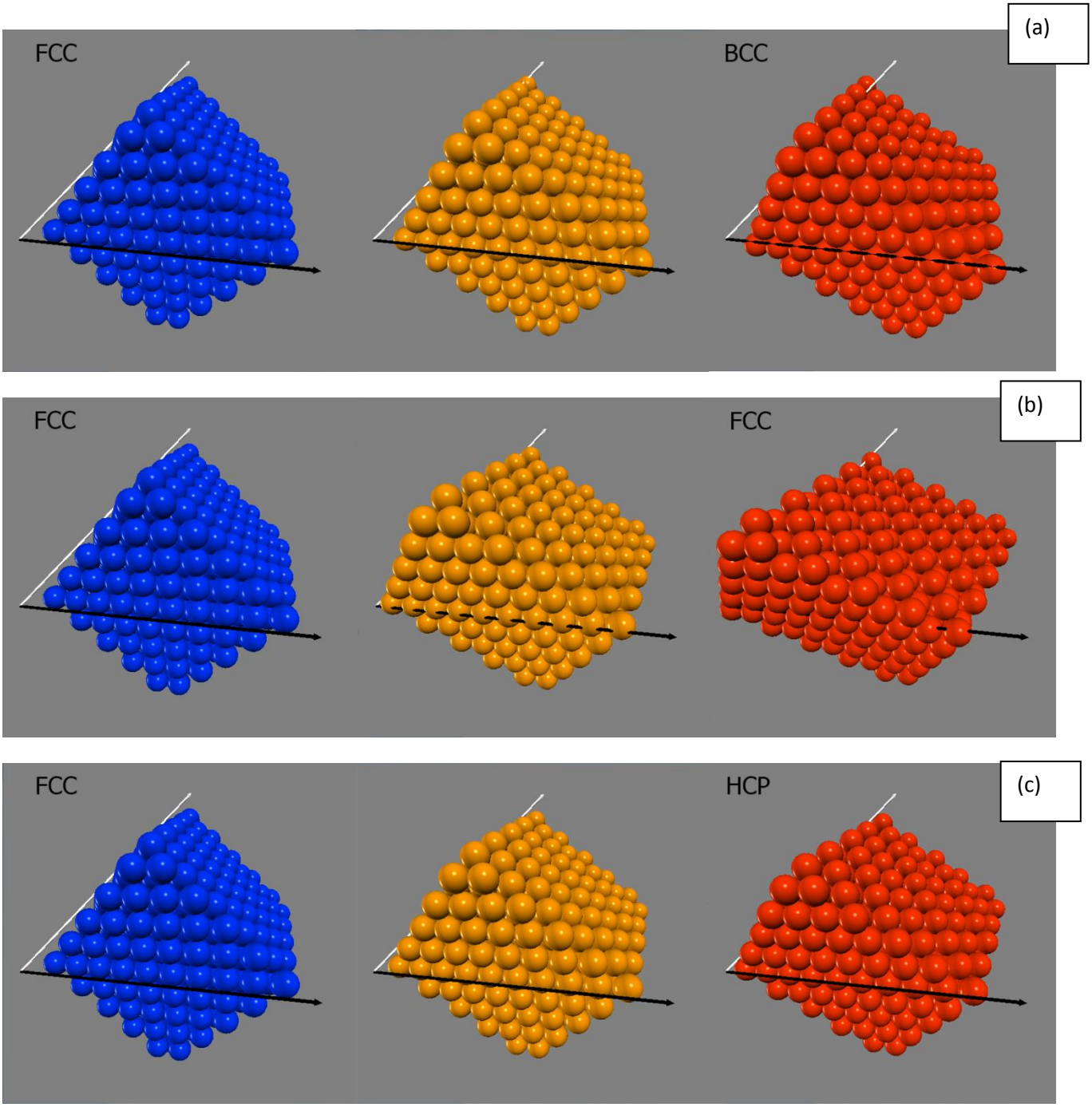

Fig. 4. *3D representations of (a) fcc→ bcc martensitic transformation, (b) fcc→ fcc mechanical twinning, and (c) fcc→ hcp martensitic transformation, with, in blue, the initial parent fcc cube with its* $\{100\}_\gamma$ *facets, in red, the resulting transformed daughter crystals, and in yellow, the intermediate states stopped at medium path (half of the maximum distortion angle). The black arrow represents the invariant neutral line* $[110]_\gamma$*, and the white arrow the* $[101]_\gamma$ *direction (also invariant for the fcc→ hcp and fcc→ fcc transformations).*

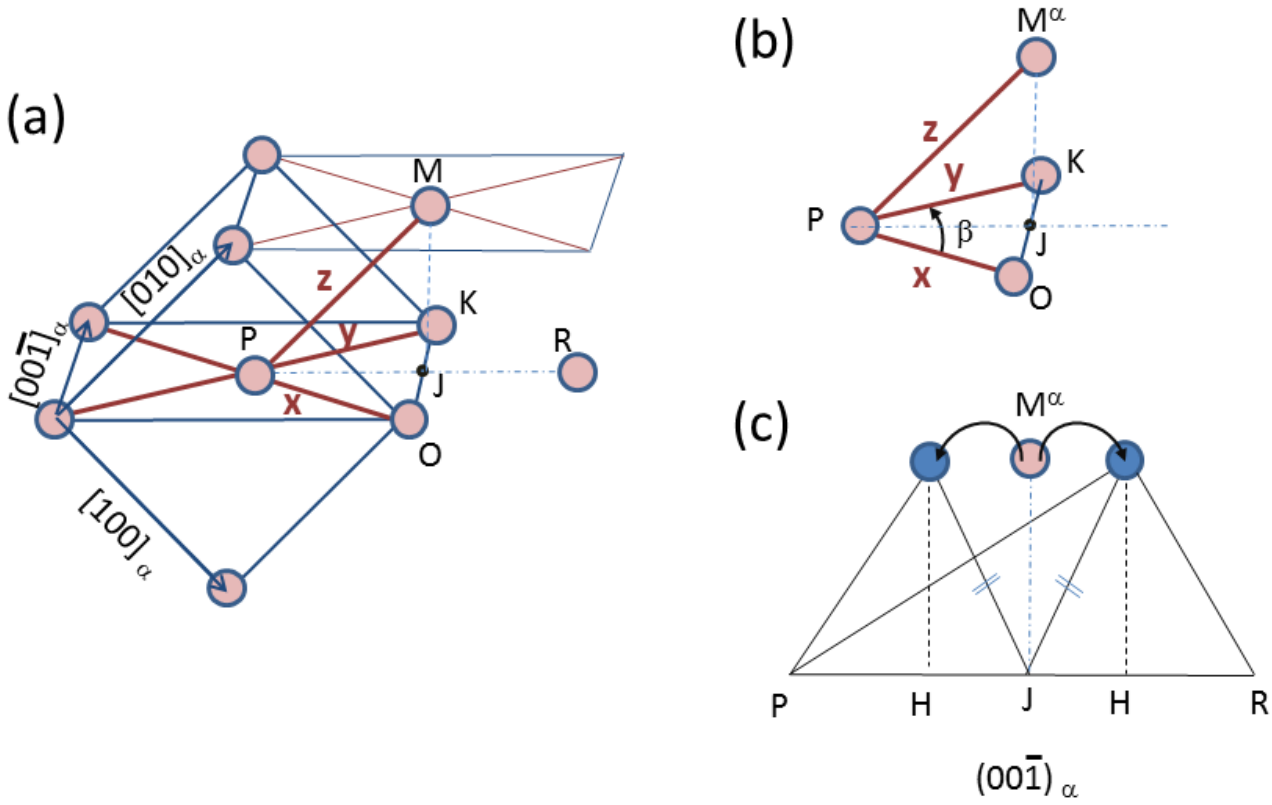

Fig. 5. *Lattice used for the bcc→fcc and bcc→hcp transformations. (a) The triangle POK corresponds to the same triangle as used for the fcc→bcc transformation. The directions PO and PK are the close-packed directions* ***PO*** *= ½ [111]* $_\alpha$ *and* ***PK*** *= ½ [11*$\bar{1}$*]* $_\alpha$*. (b) The angle β between these two directions changes from β = 70.5° (bcc) to β = 60° (fcc). In the final state (fcc), the atoms O and K are in contact. The atom M is such that* ***PM*** *= [010]* $_\alpha$*. The projection of M on the plane POK = (*$\bar{1}$*10)* $_\alpha$ *is J such that in the bcc structure* ***JM*** *= ½ [*$\bar{1}$*10]* $_\alpha$*. (c) During the bcc →fcc transformation, the atom of the bcc phase initially in position* M^α *shuffles to the position* M^γ *of the fcc phase. The shortening of the distance OK is not visible in (c) because it is perpendicular to PJ. Two equivalent shuffles in opposite directions are possible.*

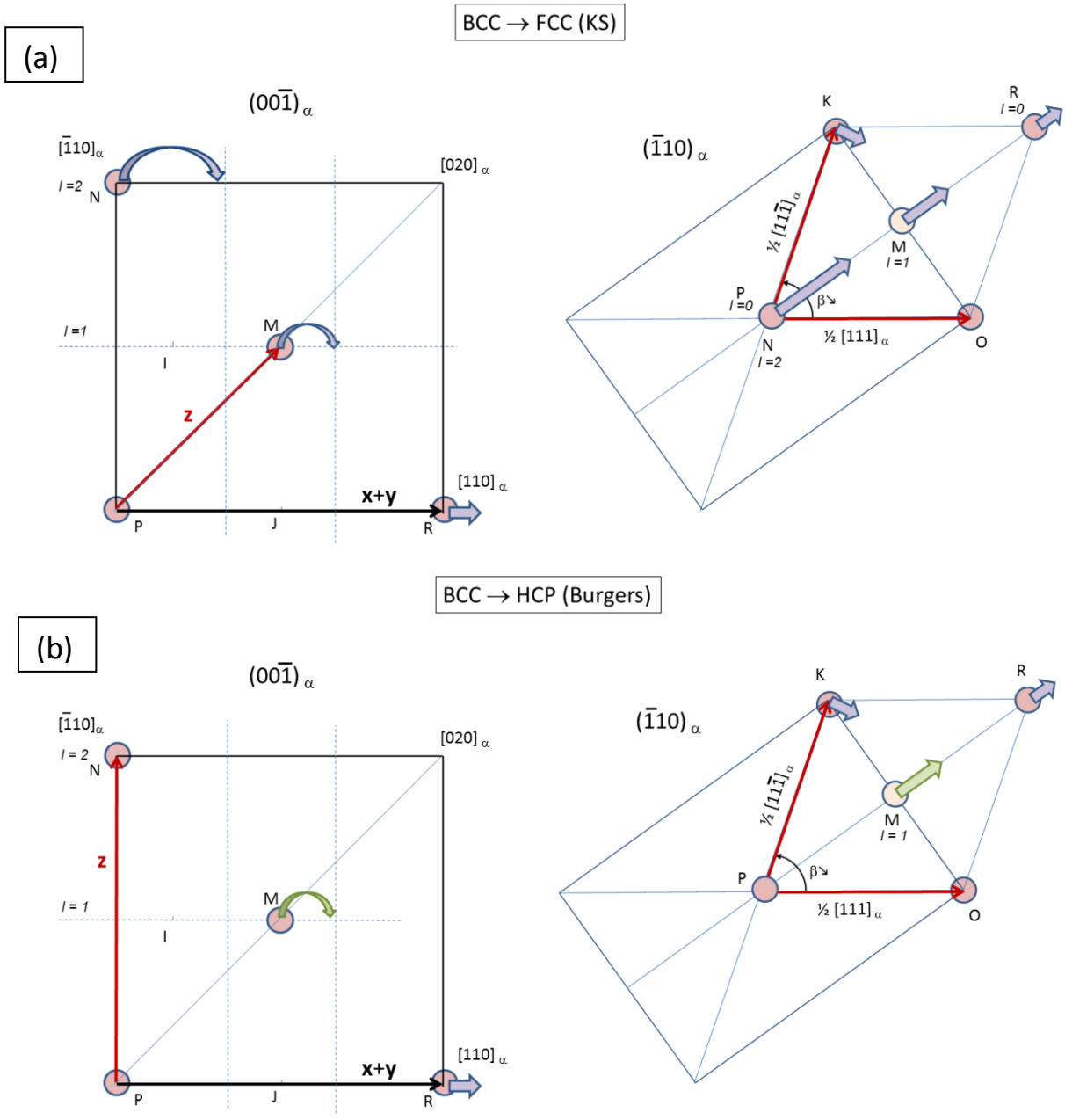

Fig. 6. *Views on the* $(00\bar{1})_\alpha$ *and* $(\bar{1}10)_\alpha$ *planes of the transformation of a bcc crystal into (a) fcc or (b) hcp crystal, with KS or SN OR, respectively. The purple arrows correspond to the atomic displacements that follow the lattice distortion, and the green arrow in (b) is a shuffle. Only one of the two possible shuffles is represented in (b). The atom in M could also have moved in the opposite direction, as shown in Fig. 5c.*

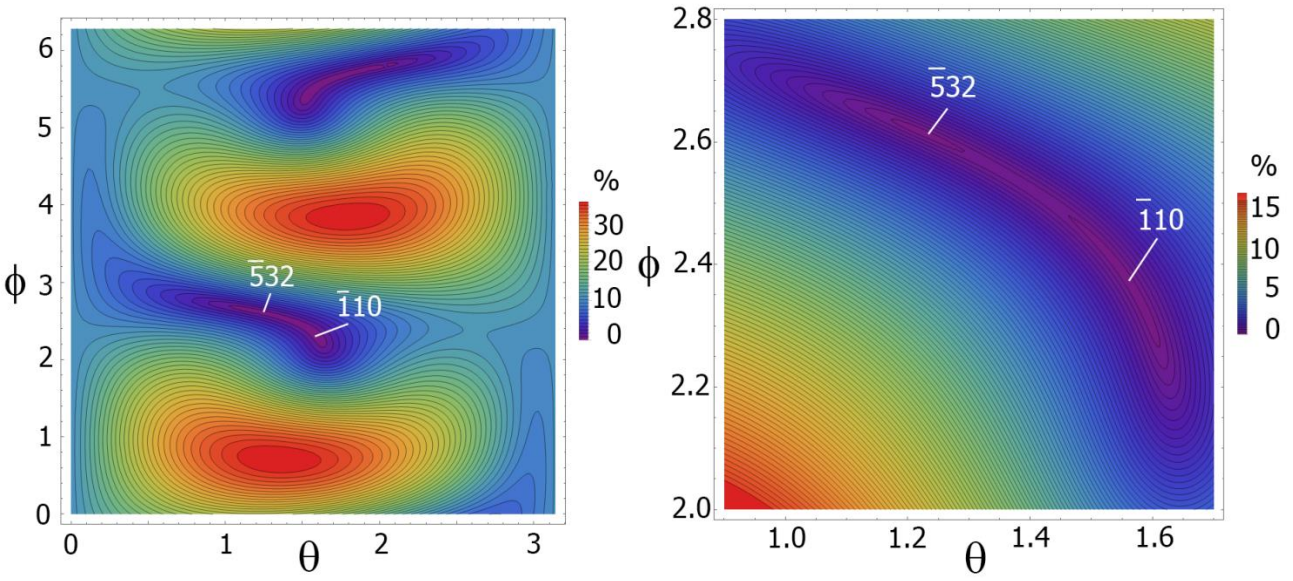

Fig. 7. *Determination of the untilted planes of the bcc→fcc transformations. (a) Graphical representations of* $\| \boldsymbol{\Delta g}_{\perp} \|$ *given in %. (a) 2D representation according to the spherical coordinates θ and φ, with* $\theta \in [0,\pi]$ *and* $\theta \in [0,2\pi]$*. (b) Enlargement of the region around the two local minima* $(\bar{1}10)_{\alpha}$ *and* $(-7-2\sqrt{6},\ 2+2\sqrt{6},\ 5)_{\alpha} \approx (\bar{5}32)_{\alpha}$.

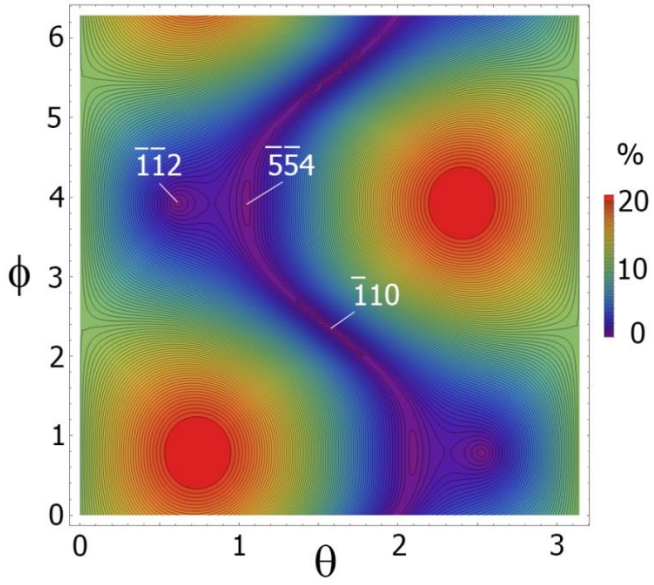

Fig. 8. *Determination of the untilted planes of the bcc→hcp transformation. (a) Graphical representation of* $\| \boldsymbol{\Delta g}_{\perp} \|$ *given in %. (a) 2D representation according to the spherical coordinates θ and φ, with* $\theta \in [0,\pi]$ *and* $\theta \in [0,2\pi]$*. The local minima* $(\bar{1}10)_{\alpha}$ *,* $(\bar{1}\bar{1}2)_{\alpha}$ *and* $(-\sqrt{6},\ -\sqrt{6},\ 2)_{\alpha} \approx (\bar{5}\bar{5}4)_{\alpha}$.

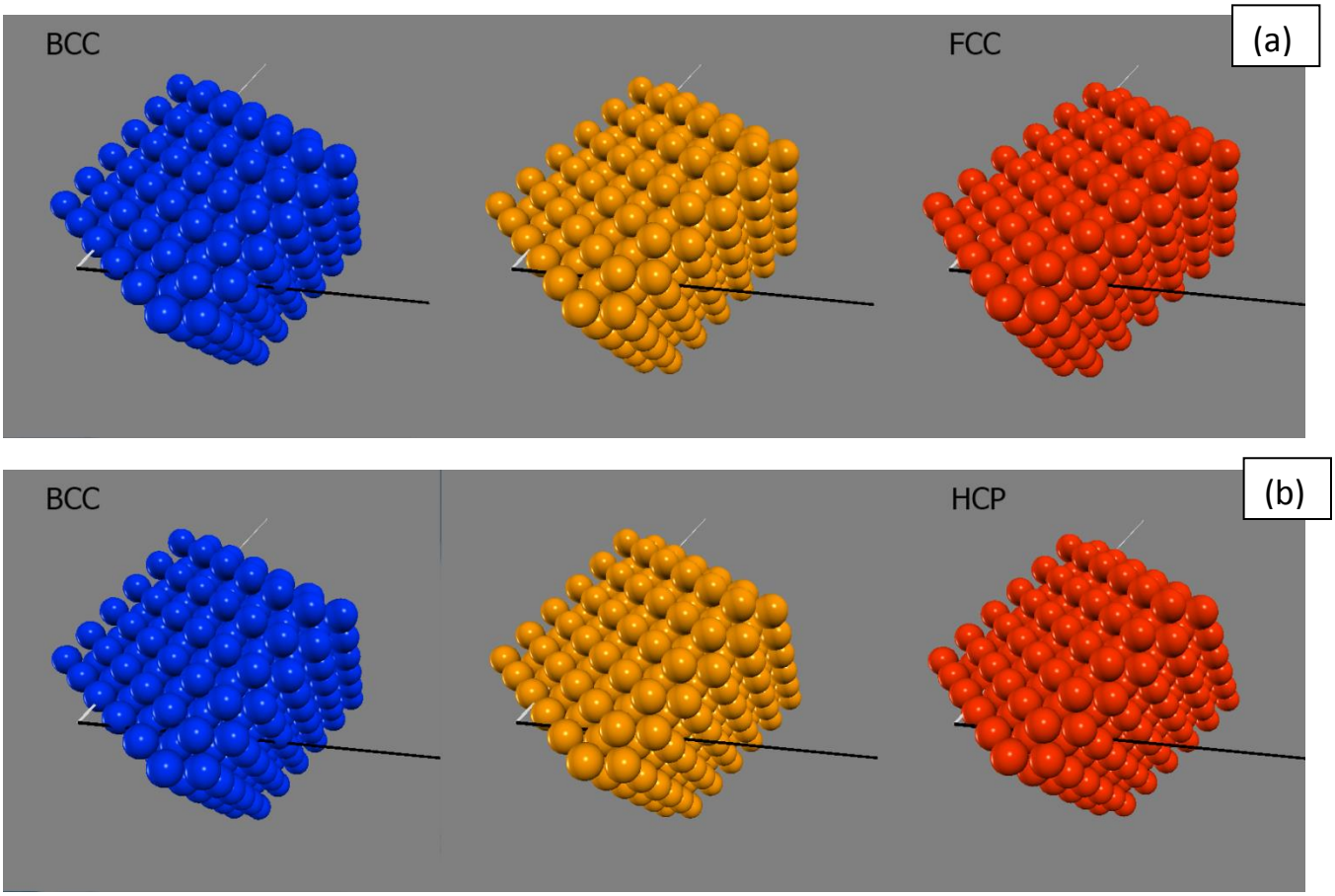

Fig. 9. *3D representations of (a) bcc→fcc and (b) bcc→hcp transformations, with, in blue, the initial parent bcc crystal cube with its* $\{100\}_\alpha$ *facets, in red, the resulting transformed daughter crystals, and in yellow, the intermediate states stopped at medium path (half of the distortion angle). The black arrow represents the invariant neutral line* $[111]_\alpha$*, and the white arrow the* $[11\bar{1}]_\alpha$ *direction (rotated by both transformations).*

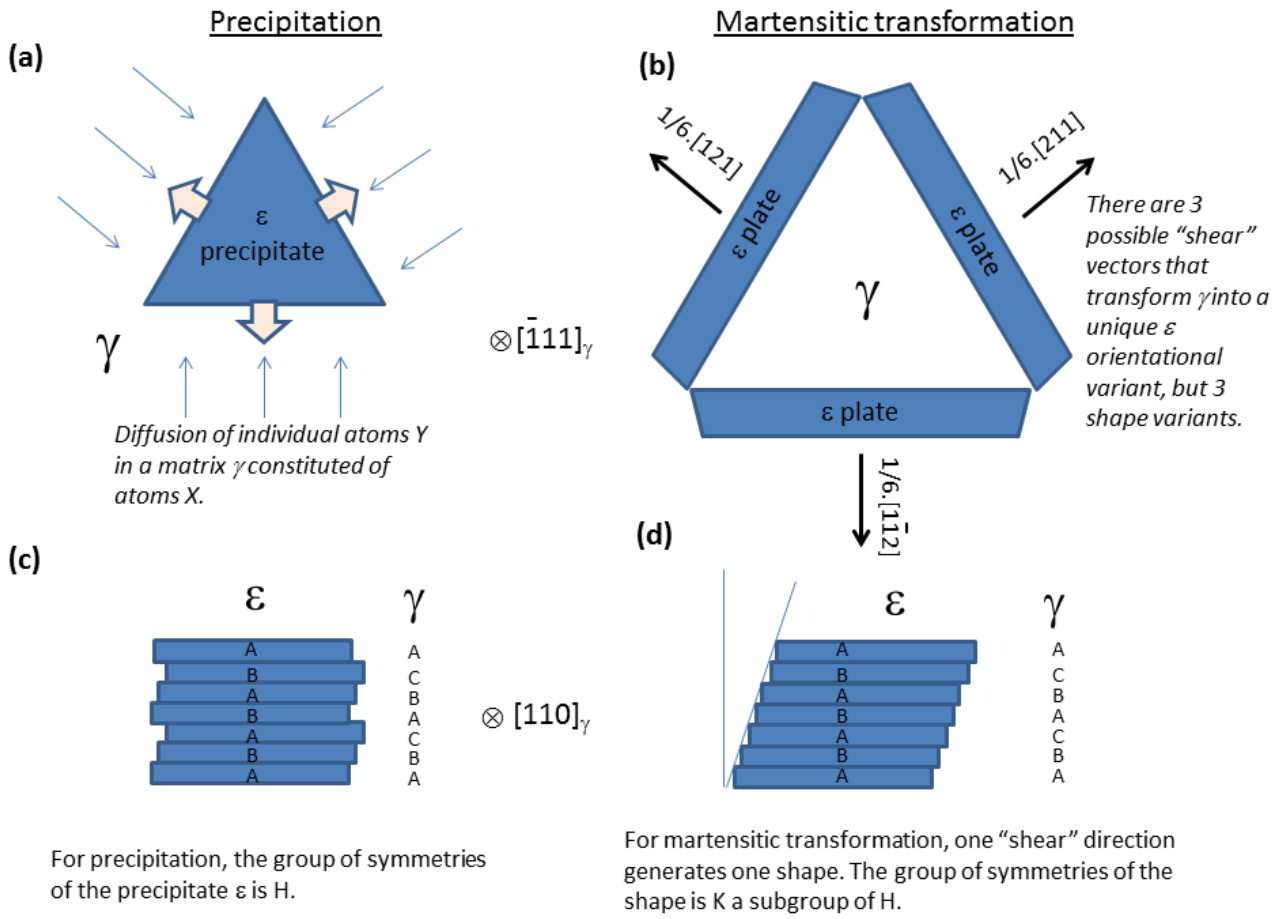

Fig. 10. *Difference of fcc→hcp transformation mechanism between (a,c) precipitation and (b,d) martensitic transformation. The schematic representations are oriented edge-on along* $[\bar{1}11]_\gamma$ *in (a,b), and on the side along* $[110]_\gamma$ *in (b,d). The point group of the shape of the precipitates is* ***H****. The point group of the shape of the martensitic variants is* ***K****; it is a subgroup of* ***H****.*

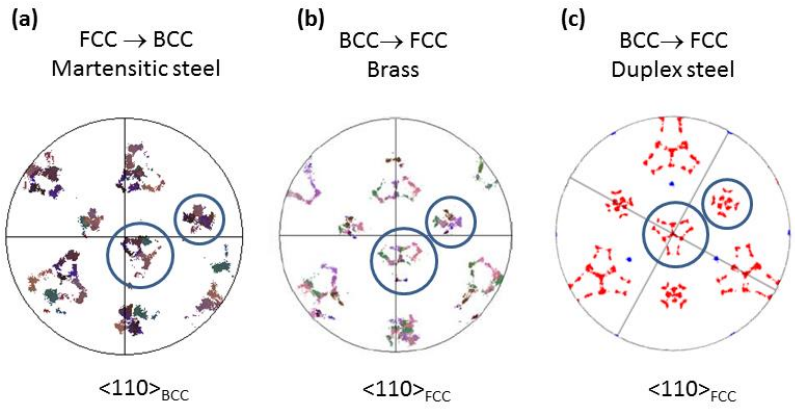

Fig. 11. *Similarities of the continuous features observed in the EBSD pole figures of (a) the* $<110>_{bcc}$ *directions formed by the martensitic laths in a parent fcc grain of a martensitic steel (EM10, thermally treated), (b) the* $<110>_{fcc}$ *directions formed by the laths of a Widmanstätten colony in a parent bcc grain of a brass alloy (from [36]), and (c) the* $<110>_{fcc}$ *directions formed by the martensitic austenite laths in a parent* δ *bcc grain, in a duplex steel (from[69]). The three-fold "flower" and four-fold "cross" are identified by the large and medium size circles.*

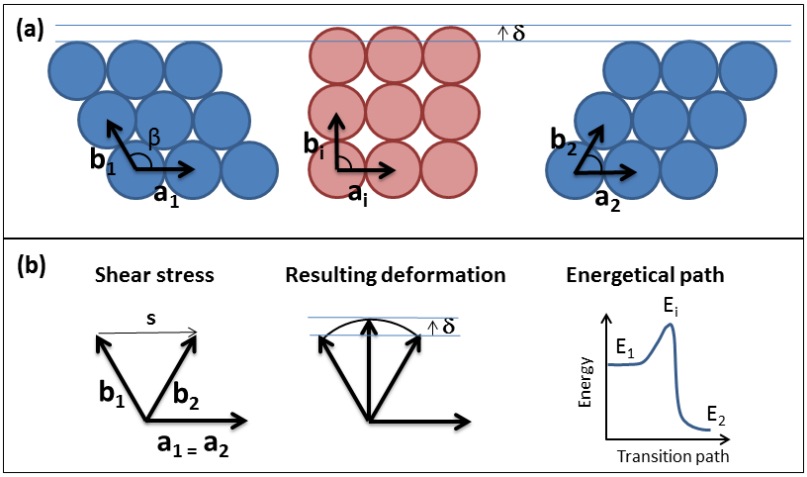

Fig. 12. *Schematic 2D representation of the intermediate states and steric barriers. (a) The* $(\boldsymbol{a}_1,\boldsymbol{b}_1)$ *basic vectors of the lattice 1 are transformed by twinning into the* $(\boldsymbol{a}_2,\boldsymbol{b}_2)$ *basic vector of the lattice 2 by the application of a shear stress* $\boldsymbol{s}$*. (b) Due to the hard-sphere packing the resulting deformation is not a simple shear strain but an angular distortion, and a slight dilatation component* $\boldsymbol{\delta}$ *naturally appears during the transformation; it is maximum in the intermediate state in red.*

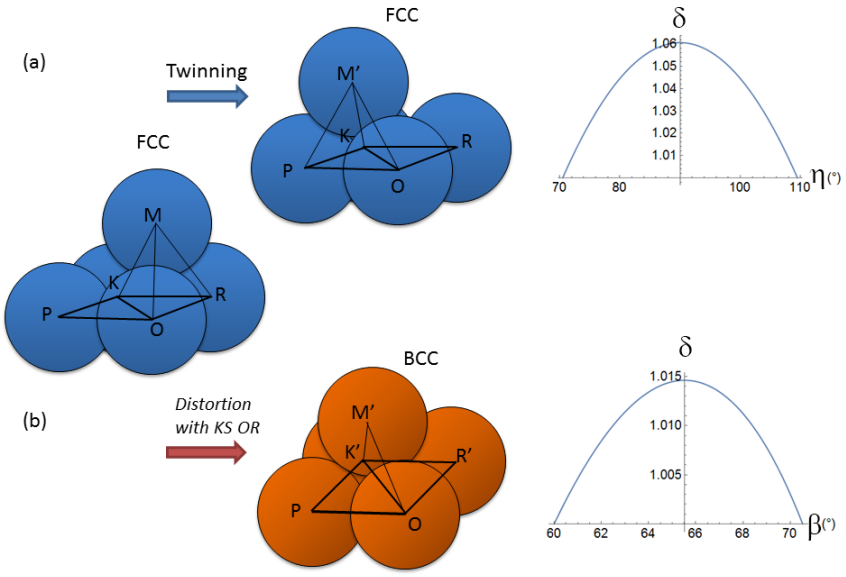

Fig. 13. *Comparison between (a) martensitic transformation and (b) twinning, with a 3D representation of the hard-sphere atoms. The letters P, O, K, M are at the centres of the atoms, as in ref. [2]. The curves at the right side represent the variation of the spacing of the* $(\bar{1}11)_\gamma$ *plane during the transformation, i.e. when the angular order parameter changes from* $\beta = 60°$ *to* $70.5°$ *for martensite, and from* $\eta = 70.5°$ *to* $109.5°$ *for twinning.*

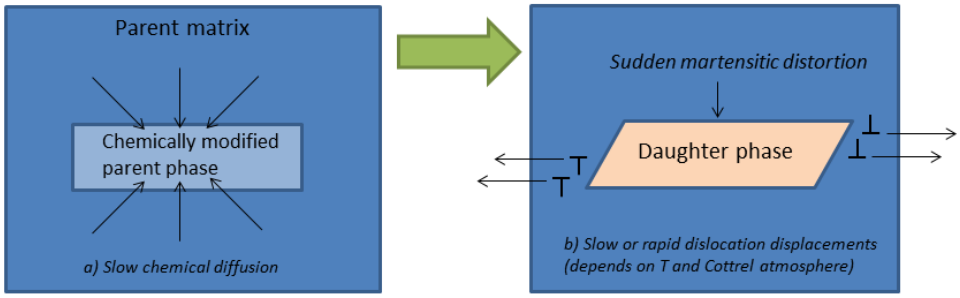

Fig. 14. *Schematic representation of a diffusion-limited displacive transformation. First, the chemical composition of the daughter phase is obtained by a slow process of atomic diffusion, but the crystallographic structure is still the parent phase one, and then, when the critical size is reached, the transformation suddenly (and displacively) occurs. The distortion introduces dislocations in the surrounding parent matrix. The kinetics of the displacements of these dislocations created at the tip of the plate can also influence the kinetics of transformation.*